DRD Line No. SE-6

DOE/JPL-955164 79/2
Distribution Category UC-63

(NASA-CR-158848) DEVELOPMENT OF ECONOMICAL IMPROVED THICK FILM SOLAR CELL CONTACT Final Report, Sep. 1978 - Apr. 1979 (Ross (Bernd) Associates) 74 p HC A04/MF A01 CSCL 10A G3/44

N79-28723

Unclas
31611

DEVELOPMENT OF ECONOMICAL IMPROVED THICK FILM SOLAR CELL CONTACT

BERND ROSS

BERND ROSS ASSOCIATES
2154 Blackmore Court
San Diego, CA 92109

FINAL REPORT

September 1978 - April 19

April 1979

Contractual Acknowledgement

The JPL Low-Cost Silicon Solar Array Project is sponsored by the U. S. Department of Energy and forms part of the Solar Photovoltaic Conversion Program to initiate a major effort toward the development of low-cost solar arrays. This work was performed for the Jet Propulsion Laboratory, California Institute of Technology by agreement between NASA and DOE.

DRD Line No. SE-6

DOE/JPL-955164 79/3
Distribution Category UC-63

DEVELOPMENT OF ECONOMICAL IMPROVED THICK FILM SOLAR CELL CONTACT

BERND ROSS

BERND ROSS ASSOCIATES
2154 Blackmore Court
San Diego, CA 92109

FINAL REPORT

September 1978 - April 1979

April 1979

Contractual Acknowledgement

The JPL Low-Cost Silicon Solar Array Project is sponsored by the U. S. Department of Energy and forms part of the Solar Photovoltaic Conversion Program to initiate a major effort toward the development of low-cost solar arrays. This work was performed for the Jet Propulsion Laboratory, California Institute of Technology by agreement between NASA and DOE.

TABLE OF CONTENTS

LIST OF FIGURES

1.0 SUMMARY

Materials were surveyed to provide candidates for an all metal electrode paste system. These consisted of a major constituent metal powder, a low melting metal powder suitable for a liquid phase sintering medium, and a powder material suitable as an etchant for silicon dioxide at sintering temperatures. By means of thermal gravimetric analysis a suitable binder was identified for low temperature fired inks.

The all metal ink concept was first demonstrated with the silver system to avoid the problems of limited process windows encountered with base metal systems.

A number of solid materials capable of selectively etching silicon dioxide at modest temperatures were identified. One of these, silver fluoride, yielded very good results, wetting the silicon surface after removing a thick (3000Å) silica layer.

Silver pastes made from silver and silver fluoride were prepared and screened onto silicon substrates. The resulting contact had excellent adhesion, scratch resistance, solderability and leach resistance, even after one hour boil in DI water. Metallurgically contacts appeared equivalent in grain structure to commercial inks containing glass frits and fired at the same temperatures. Sintering action appears to be aided by the finely divided silver metal resulting from the silver fluoride dissociation. Gross penetration into the silicon surface, as checked with electron micrography, did not appear to be a problem. The metallurgical properties of the

contact were maintained by silver fluoride additives as low as 2 wt%.

Lead powder proved to work well as a liquid sintering medium for silver, with adequate structure resulting from firing temperatures as low as 500°C. A total of 61 pastes have been prepared.

Electrically the above contacts represented leaky Schottky barriers on 4-5Ωcm N-type and 1-2Ωcm P-type silicon. Barrier heights were estimated at 0.72 eV from C-V plots. An Auger electron analysis of the contact including the silver-silicon interface did not show any fluorine compounds. Doping reduced the effective contact resistance, but appeared to require higher temperatures than was needed for structural and metallurgical considerations. Best results on P-type substrates were obtained by addition of eutectic powder of aluminum-silicon, aluminum-germanium and aluminum-germanium:gallium. The results suggest further experimentation with eutectic additives to enable formation of a thin highly doped regrowth layer.

2.0 INTRODUCTION

The potential for economy and efficiency has been demonstrated for the thick film metallization process using screen printing for solar cell electrodes. However, process reliability and materials economy remain deficient. It is believed that these deficiencies can be removed by the use of ink formulations designed specifically for silicon solar cells, departing from ceramic technology tradition and utilizing all metal systems. The objectives of this investigation are as follows:

1. Eliminate the glass frit which has been the conventional liquid phase sintering medium and adhesive for metallization inks.

2. Provide an appropriate metal which can serve as the liquid phase sintering medium.

3. Find a chemical constituent which effectively removes the native oxide from the silicon during the firing step, which can be made part of the ink, and which either becomes fugitive or remains an inert part of the matured metallization.

4. Maintain cognizance of the cost objectives of the LSA Project in selecting materials and processes.

3.0 METAL SYSTEMS CONSIDERATIONS

A large number of phase diagrams of binary metal systems were examined. Several systems were selected as potential candidates based upon conductivity, compatibility with silicon, processing ease, solderability and cost. Process factors included mutual solubilities, temperature requirements and toxicity. Solubility curves were plotted from the phase diagrams for several systems. Metal system candidates included copper/tin, copper/zinc, nickel/zinc, cerium/copper, cerium/nickel, silver/tin, silver/lead, silver/antimony and silver/bismuth.

The requirements for good liquid phase sintering are: good wetting of the major constituent powder grains (copper, nickel or silver) by the frit metal liquid, reasonable solubility of the major constituent in the liquid metal, and generally compatible phase diagrams without intermetallics. Some solid solubility curves are plotted in Figures 1, 2 and 3. While silver in lead and copper in zinc appear well-behaved with increasing solubilities with temperature, the four experimental points given for silver in tin are puzzling and appear to indicate a retrograde solubility.

Initial experiments with base metal powders (copper-zinc and copper-tin) carried out in neutral atmospheres or forming gas showed both lacking adhesion and no sintering. This was attributed to oxide problems on silicon surfaces as well as on powder grains preventing wetting, along with excessive copper grain size. It was therefore decided to investigate SiO_2 removal and to utilize a major constituent powder with readily available optimal size ranges and

generally well-known and well-behaved properties as a test vehicle for the all metal ink system. Since silver met these objectives, it was considered the best choice.

Fig. 1
SOLID SOLUBILITY OF SILVER IN LEAD

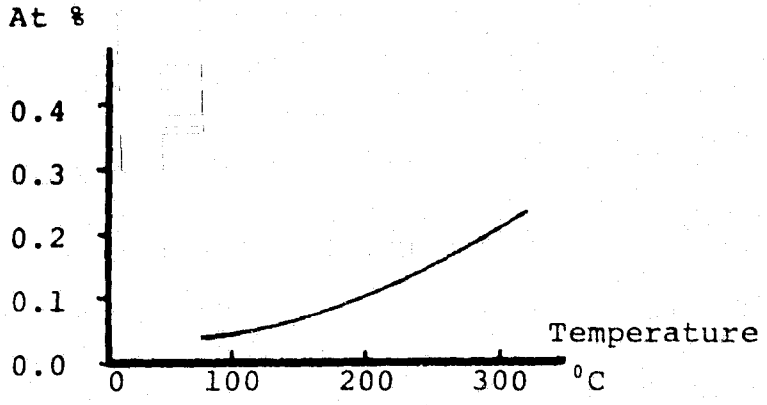

(Data taken from Ref. 1, p.38)

Fig. 2
SOLID SOLUBILITY OF COPPER IN ZINC

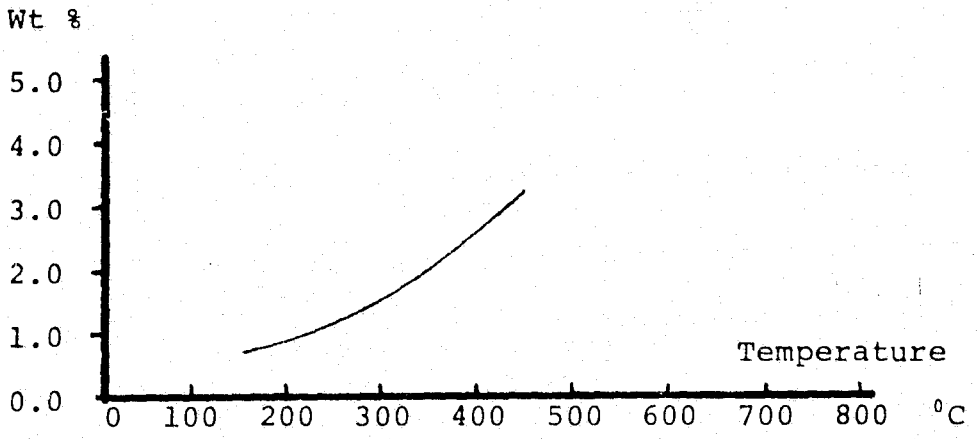

(Ibid,p. 651)

Fig. 3
SOLID SOLUBILITY OF SILVER IN TIN

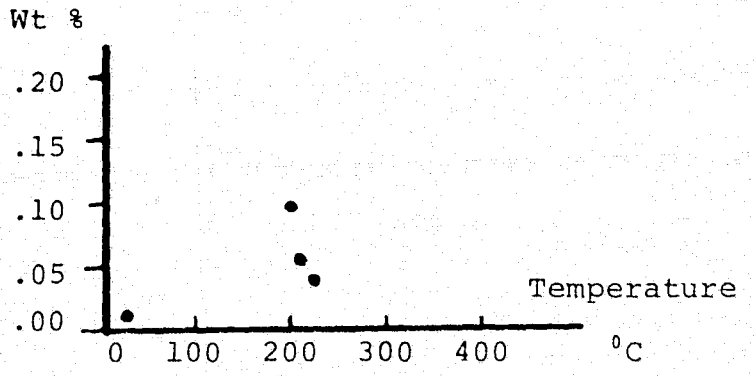

(Ibid,p.52)

4.0 METAL INK BINDER

The binder in the normal metal pastes is ethyl cellulose which has a very low volatility, with sublimation being complete only at temperatures as high as 800°C. Fortunately a proprietary, acrylic based binder was available from the subcontractor which depolymerizes at temperatures as low as 225°C. This can be seen from the combined TGA/DTA traces in Figure 4. This shows the weight loss (or gain) on the trace labeled TGA (thermal gravimetric analysis). The differential thermal analysis indicates exothermic and endothermic reactions. Normally the exothermic reactions are indicated by a positive (upward) trace excursion whereas endothermic events show a negative dip. The signal is derived from two thermocouples electrically in opposition, attached to two crucibles containing the sample, and a non-reactive reference, respectively. In the following two Figures the polarity of the thermocouples was reversed. The DTA trace of Figure 4 therefore indicates an endotherm at 230°C in coincidence with the weight loss on the TGA. The endotherm corresponds to the heat of vaporization of the binder solvent. The exotherm at 430°C would be indicative of oxidation of the sample residue.

The DTA of the silver fluoride in Figure 5 shows melting at 430°C. At 460°C another endotherm is indicated followed by an exotherm. Whether this corresponds to a multi-step dissociation process would require additional analysis beyond the scope of this program. These curves provide valuable information about the chemical and physical reactions taking place as the temperature is swept from room temperature to the desired upper limit. A check was made with this

instrument on the decomposition temperature of silver fluoride. Figure 5 shows the TGA/DTA trace. A temperature of 470°C was found for decomposition. The dip of the DTA line below the average trace at 435°C indicates melting in agreement with the literature.

PART NO. 990092

RUN NO. ___ DATE 10-6-78	T-AXIS	DTA-DSC	TGA	TMA	
OPERATOR DM	SCALE, mv/in 0.8	SCALE, °C/in 4.0	SCALE, mg/in 5.0	SCALE, mils/in	
SAMPLE: V5005 (BINDER)	PROG. RATE, °C/min 25	(mcal/sec)/in	SUPPRESSION, mg	MODE	
ATM ___ @ AIR	HEAT ___ COOL ___ ISO ___	WEIGHT, mg	WEIGHT, mg 30.0	SAMPLE SIZE	
FLOW RATE 3 CU FT/HR	SHIFT, in 0	REFERENCE	TIME CONST, sec	LOAD, g	
			dY, (mg/min)/in	dY, (10X), (mils/min)/in	

DUPONT Instruments

MEASURED VARIABLE

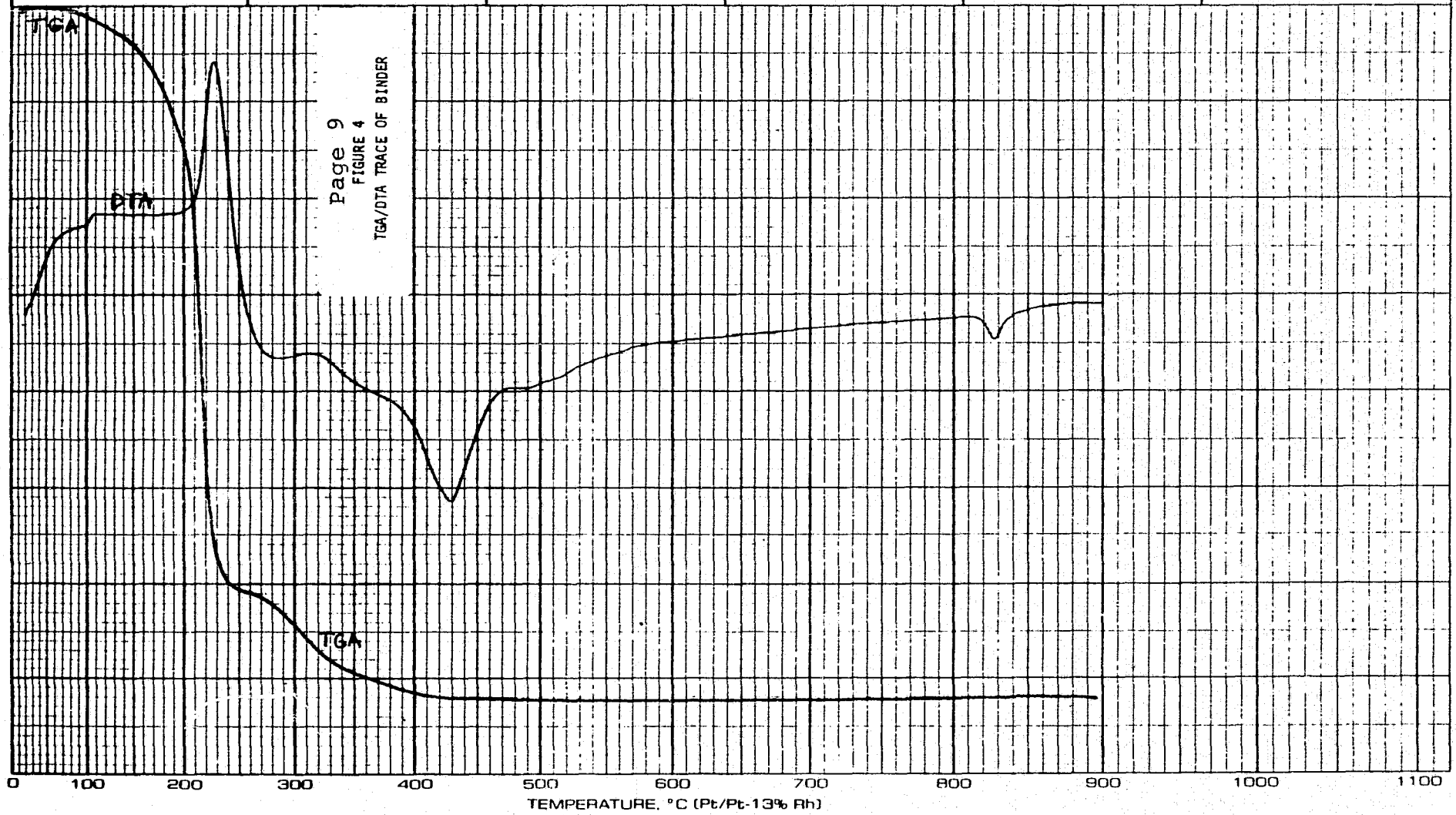

PART NO. 990092

RUN NO. ___ DATE. ___	T-AXIS	DTA-DSC	TGA	TMA
OPERATOR DM	SCALE, mv/in 0.8	SCALE, °C/in 4.0	SCALE, mg/in 5.0	SCALE, mils/in
SAMPLE: SILVER FLUORIDE AgF	PROG. RATE, °C/min 15	(mcal/sec)/in	SUPPRESSION, mg	MODE
ATM AIR @	HEAT ___ COOL ___ ISO ___	WEIGHT, mg	WEIGHT, mg 30.0	SAMPLE SIZE
FLOW RATE 3 CUFt/hr	SHIFT, in 0	REFERENCE	TIME CONST, sec	LOAD, g
			dY, (mg/min)/in	dY, (10X), (mils/min)/in

DUPONT Instruments

MEASURED VARIABLE

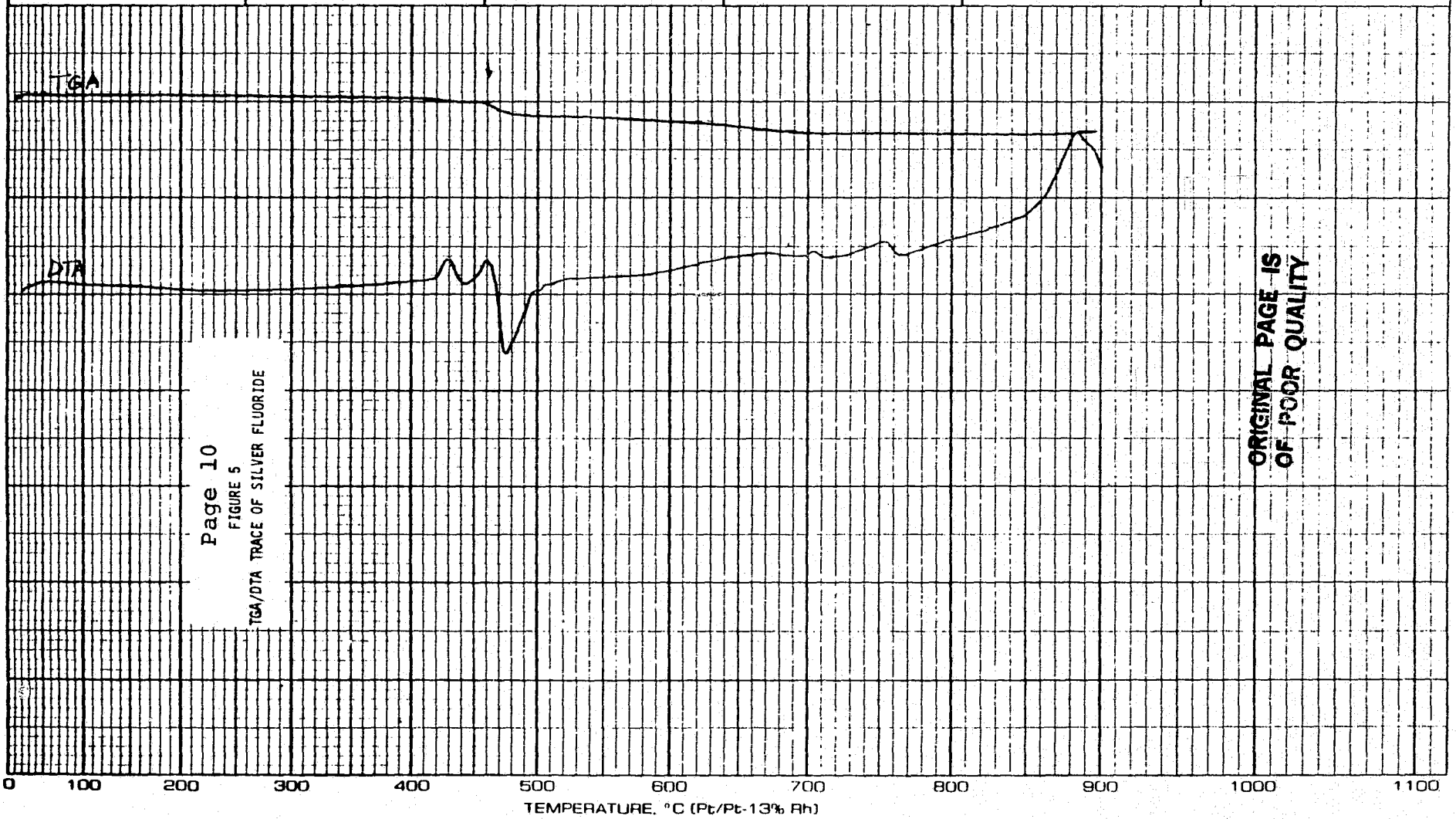

Page 10

FIGURE 5
TGA/DTA TRACE OF SILVER FLUORIDE

5.0 CONSIDERATIONS ON SILICON DIOXIDE REMOVAL

Silicon dioxide is easily removed with HF in an aqueous solution or by dry, hot fluorine, according to:

$$4\ HF + SiO_2 \rightarrow SiF_4\uparrow + 2H_2O$$

$$2F_2 + SiO_2 \xrightarrow{\Delta} SiF_4\uparrow + O_2\uparrow$$

Since the use of HF is not convenient, we looked for fluorine-containing compounds which had low decomposition or melting temperatures and could be incorporated in the metal paste. The most attractive material appeared to be silver fluoride (AgF) which according to the literature, decomposes at 435°C. Others ordered included zinc fluoride (ZnF_2), aluminum fluoride (AlF_3), ammonium fluoride (NH_4F) and ammonium bifluoride (NH_4HF_2). The metal fluoride salts are expected to decompose with the fluorine becoming fugitive in the nascent state (F), causing it to be highly reactive. The cation is left behind reduced to the metallic form and is expected to combine with the other metallic ink constituents. This reaction would go in accordance with:

$$4AgF + SiO_2 \xrightarrow{\Delta} SiF_4\uparrow + 4Ag + O_2\uparrow$$

In the ammonium salt decomposition the products are gaseous ammonia, fluorine and in the case of NH_4HF_2, anhydrous hydrofluoric acid.

Since the metallic hydrides, titanium hydride and zirconium hydride, act in a very similar manner, releasing highly reactive nascent hydrogen and leaving the metal behind, these hydrides were tried as well.

6.0 SILICON DIOXIDE REMOVAL EXPERIMENTS

Polished silicon wafers of N-type material and a resistivity of 5Ωcm were oxidized in air at a temperature of 1100°C for 30 minutes. The resulting silica layers gave uniform interference colors of reddish-purple and were estimated to be 2500Å (0.25μm) thick. Subsequent SEM photographs showed the thickness to be closer to 3000Å (0.3μm). The rationale for growing such a thick layer of SiO_2 concerns the ease with which the efficacy of an etchant material could be judged in this system. While the thickness of the native oxide is probably only a few atomic layers (10 - 20Å), it is quite difficult to determine the existence of such layers by unsophisticated means.

A small quantity of pure fluorine containing material was placed in the center of the oxidized wafer. The wafer was put on a Kulicke-Soffa bonder heater stage and observed with a binocular microscope. The heater stage was set to a pre-determined temperature. This temperature was usually about 100°C above the estimated decomposition temperature. The estimate was based upon our TGA/DTA measurements and values obtained from the literature.

7.0 AMMONIUM FLUORIDE

Figure 6 shows the TGA/DTA traces for ammonium fluoride (NH_4F). The TGA trace illustrates that weight loss occurs almost immediately, with the slope becoming quite steep at 150°C. While there are several inflection points, further emphasized by the structure apparent on the DTA trace, the weightloss is 71% complete at 250°C and 100% at 450°C. The structure exhibited in the DTA of Figure 6 is not understood. According to Berzelius[3], NH_4F melts prior to decomposition, a phenomenon not noted by other references. The same reference points out that dissociation of ammonium fluoride proceeds according to $NH_4F \rightarrow NH_3 + HF$. Similarly, the reference asserts that NH_4F will dissociate into NH_4HF_2 and $NH_3\uparrow$ in the presence of water.

Figure 7 shows an electron micrograph taken on a Cambridge SEM 1700X magnification, picturing the boundary between the virgin layer and the portion covered with ammonium fluoride. A light microscope examination showed a dark residue, whose nature remains unknown.

PART NO. 990092

RUN NO. ___ DATE 11-8-78	T-AXIS	DTA-DSC	TGA	TMA
OPERATOR DM	SCALE, mv/in 0.8	SCALE, °C/in 4.0	SCALE, mg/in ~L2	SCALE, mils/in
SAMPLE AMMONIUM FLUORIDE NH_4F	PROG. RATE, °C/min 25	(mcal/sec)/in	SUPPRESSION, mg	MODE
ATM AIR @	HEAT ___ COOL ___ ISO ___	WEIGHT, mg	WEIGHT, mg 8.5	SAMPLE SIZE
FLOW RATE 3 CU FT/HR	SHIFT, in 0	REFERENCE	TIME CONST., sec	LOAD, g
			dY, (mg/min)/in	dY, (10X), (mils/min)/in

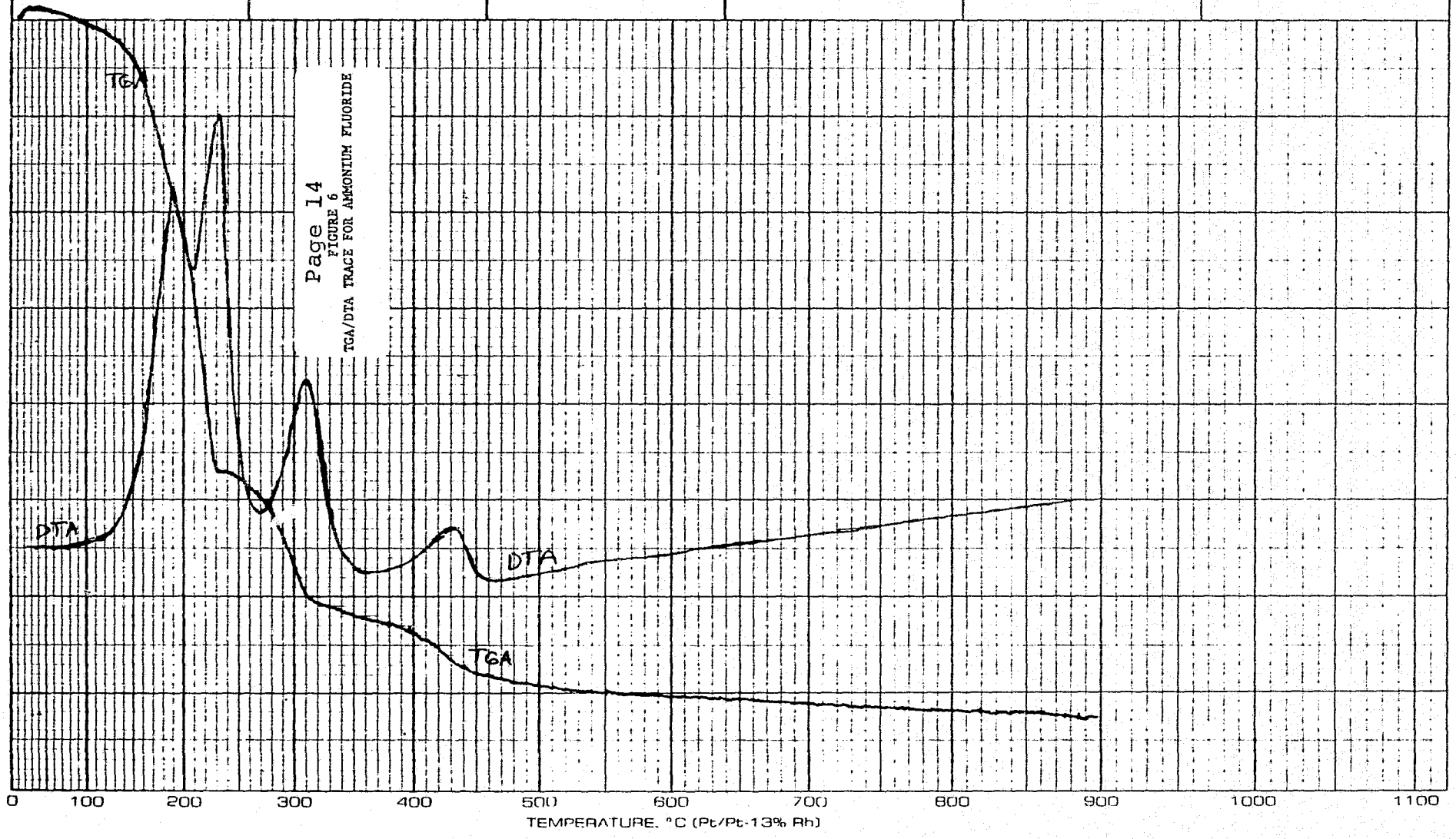

Page 14
FIGURE 6
TGA/DTA TRACE FOR AMMONIUM FLUORIDE

DUPONT Instruments

MEASURED VARIABLE

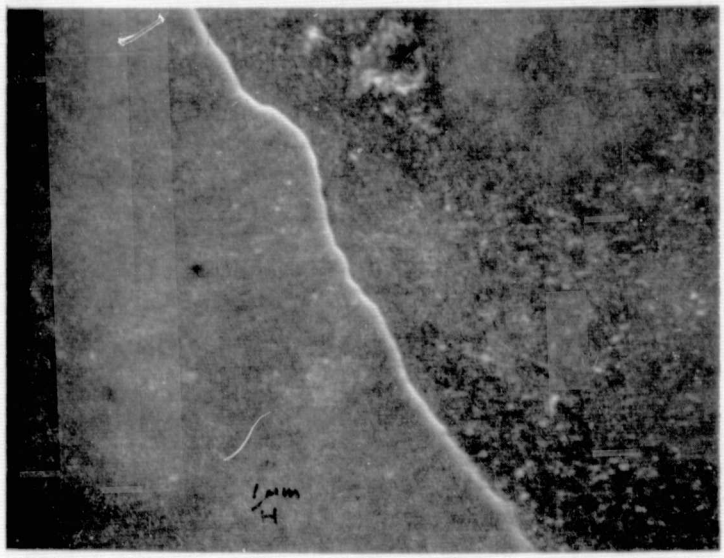

Figure 7. SiO_2 3000Å thick on silicon, left half of photomicrograph. Right portion etched by ammonium fluoride NH_4F at 600°C. Taken on Cambridge SEM at 1700X.

8.0 Ammonium bifluoride (NH_4HF_2)

Figure 8 shows the TGA/DTA traces of ammonium bifluoride to be very similar to those of ammonium fluoride. The action upon silicon dioxide was also similar, and therefore no electron micrograph is shown.

PART NO. 990092

RUN NO. ___ DATE 11-7-78	T-AXIS	DTA-DSC	TGA	TMA	
OPERATOR DM	SCALE, mv/in 0.8	SCALE, °C/in 4.0	SCALE, mg/in ~2	SCALE, mils/in	
SAMPLE: AMMONIUM BIFLUORIDE NH_4HF_2	PROG. RATE, °C/min 25	(mcal/sec)/in	SUPPRESSION, mg	MODE	
ATM AIR @	HEAT ___ COOL ___ ISO ___	WEIGHT, mg	WEIGHT, mg 12,5	SAMPLE SIZE	
FLOW RATE 3 cu ft/hr	SHIFT, in 0	REFERENCE	TIME CONST, sec	LOAD, g	
			dY, (mg/min)/in	dY, (10X), (mils/min)/in	

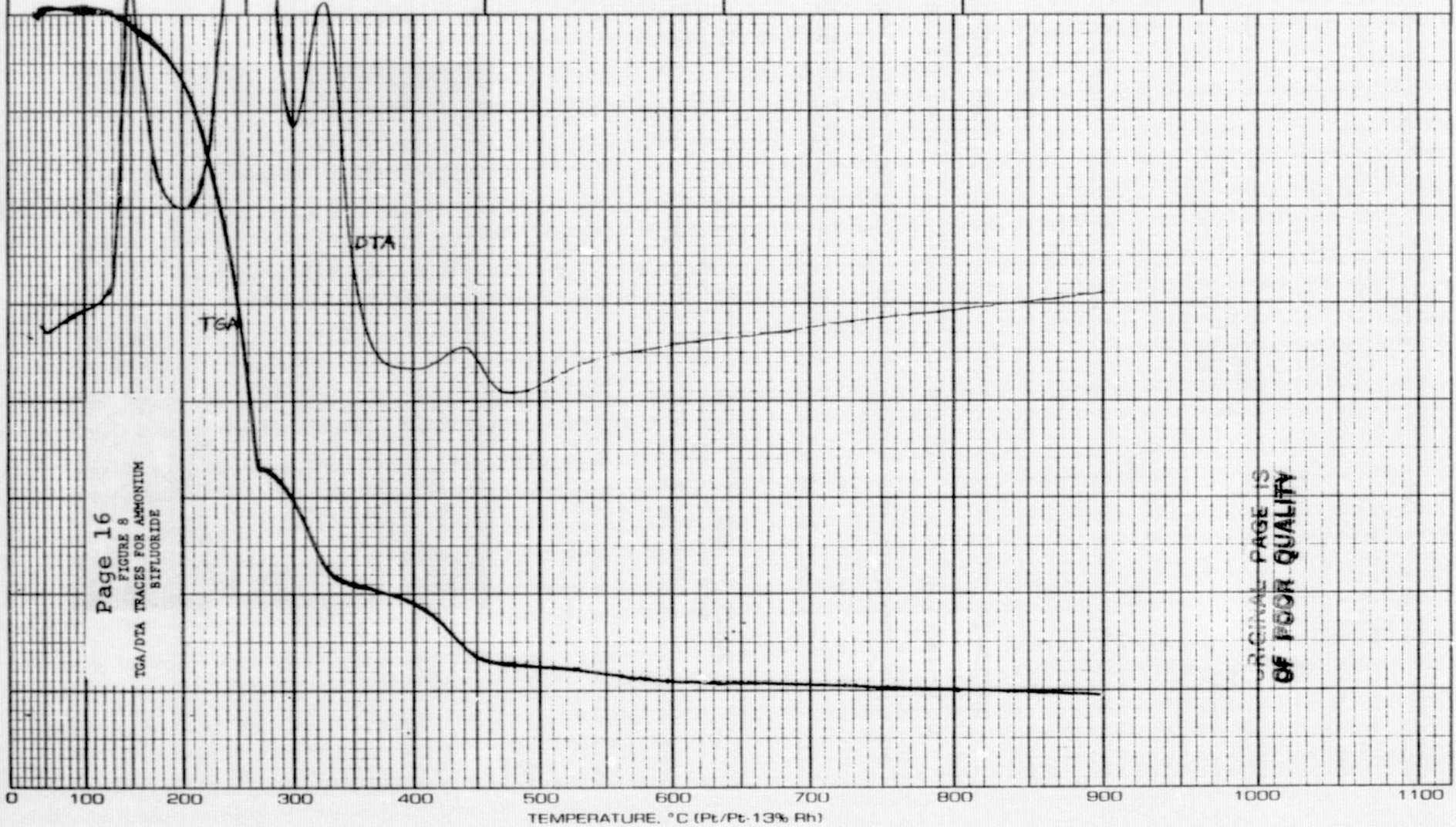

DU PONT Instruments

MEASURED VARIABLE

Page 16
FIGURE 8
TGA/DTA TRACES FOR AMMONIUM BIFLUORIDE

ORIGINAL PAGE IS
OF POOR QUALITY

9.0 TEFLON ^{R}

Figure 9 shows the TGA/DTA trace for Teflon ^{R}. The continuous rise in the TGA trace is possibly due to the aerodynamics of a different crucible, experiencing lift in the chimney of the apparatus, which would be interpreted as weightloss. Melting occurs at 320^{o}C (DTA) and decomposition is apparent from the weightloss beginning at 500^{o}C and being complete at 630^{o}C. Figure 10 is an SEM photo of the interface of the attacked versus the non-attacked portions of the oxidized wafer. Optical microscopy again revealed a considerable amount of residue. There is an indication on the SEM that the silicon surface may have been attacked as shown in the apparent cratering on the left side of the photo.

PART NO. 990092

RUN NO. ___ DATE 11-9-78	T-AXIS	DTA-DSC	TGA	TMA	
OPERATOR DM	SCALE, mv/in 0.8	SCALE, °C/in 4.0	SCALE, mg/in 5.0	SCALE, mils/in	
SAMPLE: DLX 6000 (TEFLON®)	PROG. RATE, °C/min	(mcal/sec)/in	SUPPRESSION, mg	MODE	
	HEAT ___ COOL ___ ISO	WEIGHT, mg	WEIGHT, mg 35.6	SAMPLE SIZE	
ATM AIR @	SHIFT, in 0	REFERENCE	TIME CONST., sec	LOAD, g	
FLOW RATE 3 CU FT/HR			dY, (mg/min)/in	dY, (10X), (mils/min)/in	

DU PONT Instruments

MEASURED VARIABLE

Page 18

FIGURE 9. TGA/DTA TRACES FOR TEFLON® POWDER

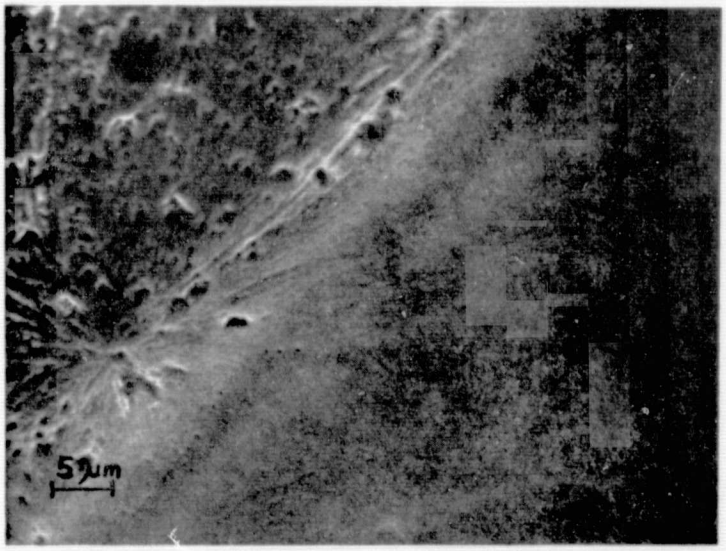

Figure 10. SiO_2 3000 Å thick on silicon, right half of photo. Left half etched by decomposed Teflon® at 600°C. Taken on Cambridge SEM at 1600X.

10.0 SILVER FLUORIDE (AgF)

Only a small quantity of silver fluoride was obtained due to its rather high price (over $6/g). It was later established that this high price is probably due to limited usage rather than material and labor costs.[4] An attempt to obtain electronmicrography of a silver fluoride grain proved to be impossible as the 10 KeV, 100μA cathode current electron beam decomposed the specimen grain in considerably less than a minute.

Figure 11 shows an SEM photo of a typical silver grain resulting from AgF dissociation at 500°C on an oxidized silicon wafer. Magnification is 4000X. It can be seen that a moat has been carved out of the silica around the original silver fluoride grain. The resulting silver blob has thinned down markedly near its periphery, making a low contact angle with the silicon, a condition expected when good wetting is demonstrated.[5] The continuous metal surface is probably due to the very fine particles generated by the decomposition of the silver fluoride, as well as the catalytic action of the freshly exposed silicon crystal surface. To verify the nature of the deposited material, a series of photomicrographs was taken at increasing magnification. The backscatter mode of the Cambridge SEM was employed, providing a higher yield of electrons from the surface of materials with a high atomic number relative to the darker background (Ag Z=47 : Si Z=14). Figure 12 shows a different portion of the same sample from which Figure 11 was taken, at 1600 X magnification. Figure 13 shows a portion of Figure 12 at 3700X magnification, again employing the backscatter mode. Figure 14 shows the same region as Figure 13 but as a silver elemental map using the L_α (2.98KeV) line X-ray

fluorescence. The open areas on the solid silver portions are due to the finite integration time utilized. The sparse number of dots, where no silver is expected, is from noise and possibly some contamination.

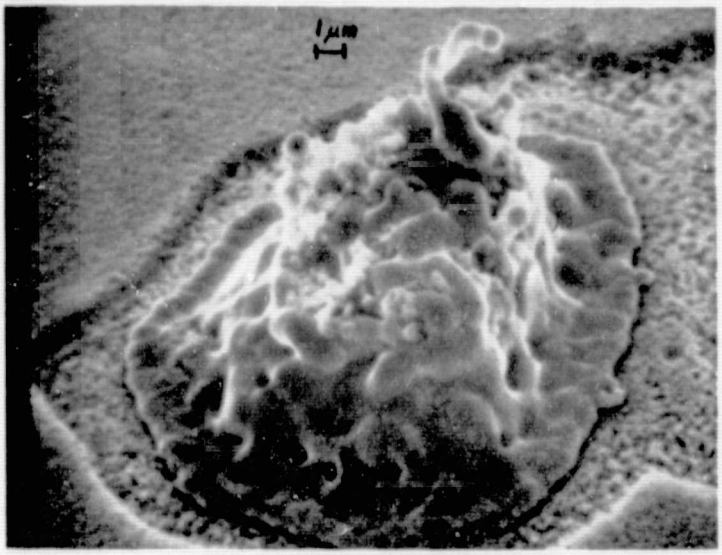

Figure 11. AgF on SiO_2 (3000 Å thick) at 500°C. Vicinity of reduced silver shows etching action on SiO_2. Good wetting is indicated by low angle of periphery profile. Cambridge SEM at 4000X.

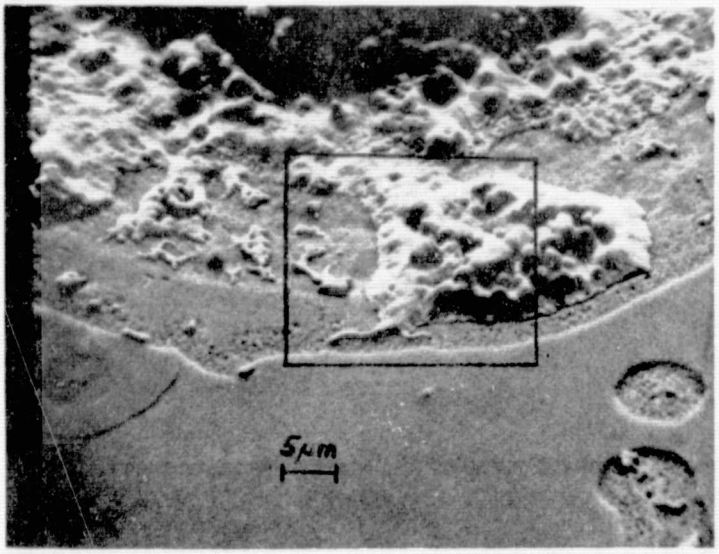

Figure 12. Different portion of same sample as above. Taken in back-scatter mode at 1500X.Cambridge SEM.

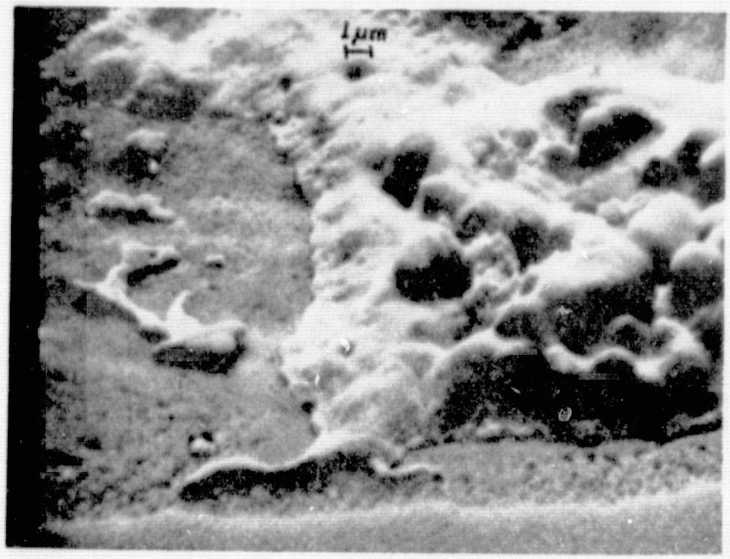

Figure 13. Same sample as Figures 12 and 11 (AgF) taken in backscatter mode on Cambridge SEM at 3700X.

Figure 14. Same sample as Figure 13 showing silver map of region above. Cambridge SEM 3700X 2.98KeV Lα. Integration time 1000 sec.

VAPOR PRESSURE OVER SILVER FLUORIDE

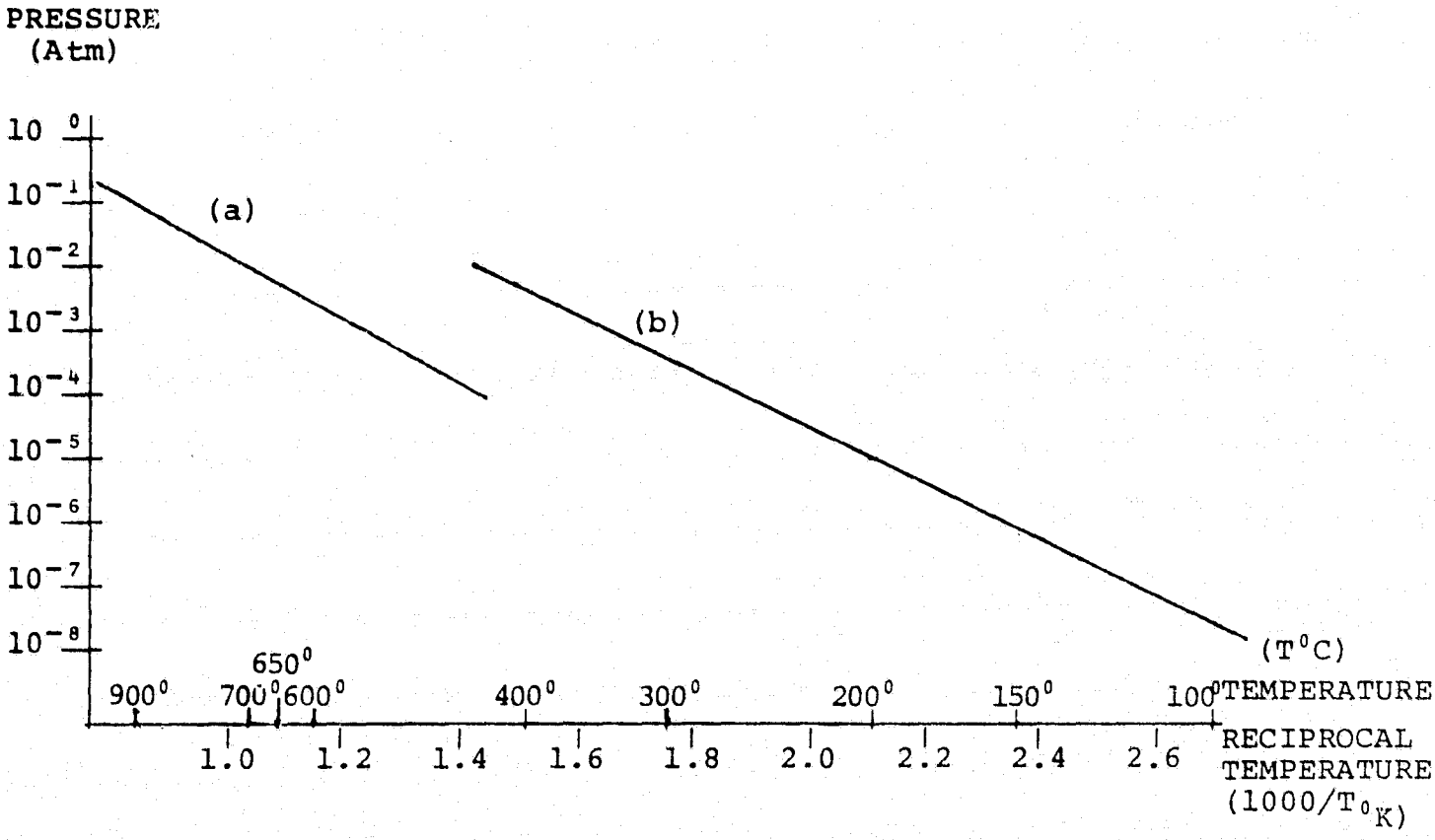

Fig.15 Vapor pressure over a) liquid silver fluoride (AgF) and b) solid silver fluoride (AgF)

(a) above liquid AgF $\quad \ln P_{atm} = -0.937 \cdot 10^4/T_{°K} + 4.78$ for $854^\circ < T < 1024^\circ K$

(experimental, from reference 6)

(b) above solid AgF $\quad \ln P_{atm} = -1.023 \cdot 10^4/T_{°K} + 10.07$ for $T \leq 708^\circ K$

(calculated, from reference 6)

Figure 15 shows the pressure in atmospheres over silver fluoride at various temperatures. The curves were plotted from the two equations[4] shown on the figure.

In addition to the above, the following were tried, all at a temperature of 600°C.

Aluminum fluoride	AlF_3
Zirconium hydride	ZrH_2
Titanium hydride	TiH_2

There was no evidence of oxide removal discernible in the above materials.

Zinc fluoride	ZnF_2

The zinc fluoride was evidently effective in removing the silicon oxide, however, it left behind a large amount of dark residue, probably ZnO. Since the other materials showed more promise, it was decided to abandon the above.

11.0 SILVER PASTE EXPERIMENTS

11.1 Initial Experiments

Sixty-one (61) different experimental pastes were fabricated (See Appendix A.2). The initial paste, consisting of 5 wt.% AgF and 95 wt.% silver powder of particle size ∿0.1μm gave good results, but had poor initial rheological properties and continued to deteriorate. This was most likely a function of the extremely small particle size which provides a large area of grain surface. This, in turn, reduces the lubricating action of the resin binder causing the viscosity to increase.

Subsequently, a coarser silver consisting of powder and flakes was used and a masterpaste was compounded. The masterpaste contains the normal ingredients of metal powder and binder and allows the rapid preparation of a series of pastes to which only the silicon oxide scavenger, as well as other experimental components including dopants, are added.

Inks containing ammonium fluoride, bifluoride and Teflon ^{R} had inadequate adhesion at all temperatures tried (600^{o}C to 750^{o}C). The criterion was our ability to scrape the electrode off with a single-edged razor blade. In another test, 0.1" squares were coated with 63-37 tin lead solder. Leach resistance was good and all samples were quickly wetted with solder. However, the Teflon ^{R} additive electrodes could be pried off the wafer after soldering, in contrast to the silver fluoride electrodes. Coverage of the silver fluoride compounded electrodes looked good.

Figures 16, 17, 18 and 19 show a sequence of SEM photos of S012 ink paste prepared with 10 wt.% added AgF fired at 750°C for five minutes. Figure 16 was done at the low magnification of 17X; Figure 17: 420X magnification; Figure 18: 1700X magnification; Figure 19: 4200X magnification. The ridges on the print in the Figures 16 and 17 are due to the paste rheology. It should be noted that the addition of Teflon ^{R} powder had a beneficial effect upon the ink rheology. Figures 18 and 19 show that there is a considerable sintering action in this all metal ink even though no liquid phase sintering medium was used. This may be due to the finely divided silver particles from the AgF dissociation.

On the other hand there is considerably less visible wetting action in these photos. It is plausible that wetting occurs under the grains and the tenacious adhesion tends to support this view.

It is interesting to compare the sintering action obtained in this experiment with that on a production solar cell (Figure 20) employing a commercial lead oxide based glass frit ink. The magnification of the glass frit sample is almost twice that of the all metal system (8000X : 4200X) and the grain development and interlocking are excellent. The firing temperatures of the two inks are comparable. (All metal ink: 750°C, commercial fritted ink 700°C.)

In order to eliminate the Schottky barrier referred to in the next section under electrical measurements, a paste (S018) was prepared containing 3 wt.% boric acid (H_3BO_3) in addition to 5 wt.% silver fluoride (AgF) and screened onto P-type wafers of 1 to 3 Ωcm solar

cell material. The resistance measurement indicated the barrier to be attenuated (refer to electrical measurements). Subsequently, a wafer with the boron containing ink along with an identical screened contact except for the boron addition (S009) was boiled in de-ionized water for one hour. Both wafers were then subjected to an adherence test involving an Exacto knife. The contact with the H_3BO_3 addition could be scraped off with little difficulty whereas the "undoped" contact survived the test.

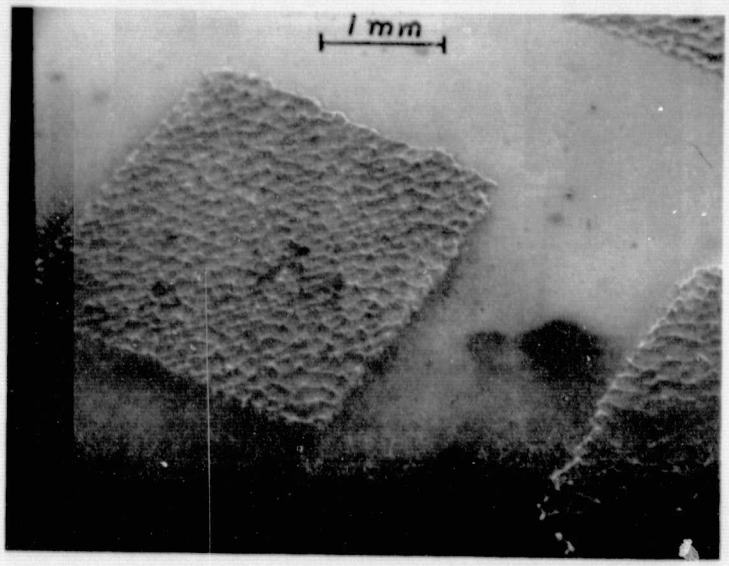

Figure 16. Print with SO12 (10% AgF). Pads are 0.100" X 0.100" spaced 0.050", on polished silicon. Fired at 750^{0}C temperature peak for 5 min. Cambridge SEM at 17X.

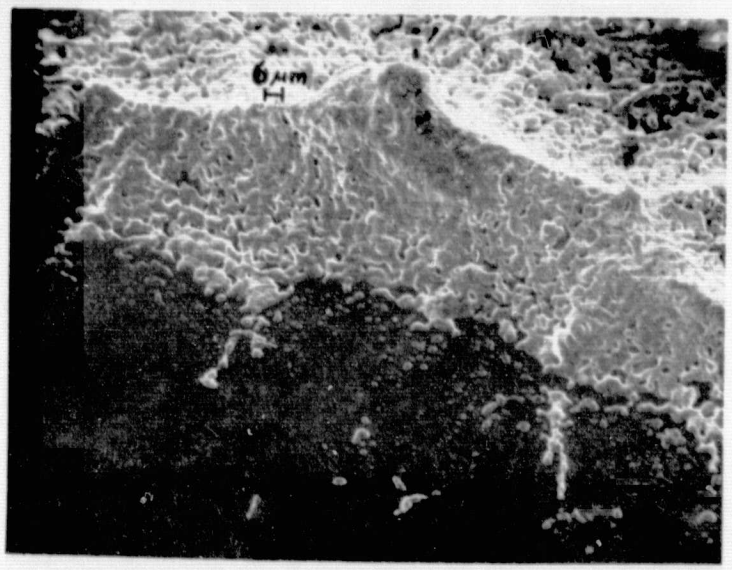

Figure 17. Same as Figure16 magnification 412X. Ridges are reproduction of screen mesh.

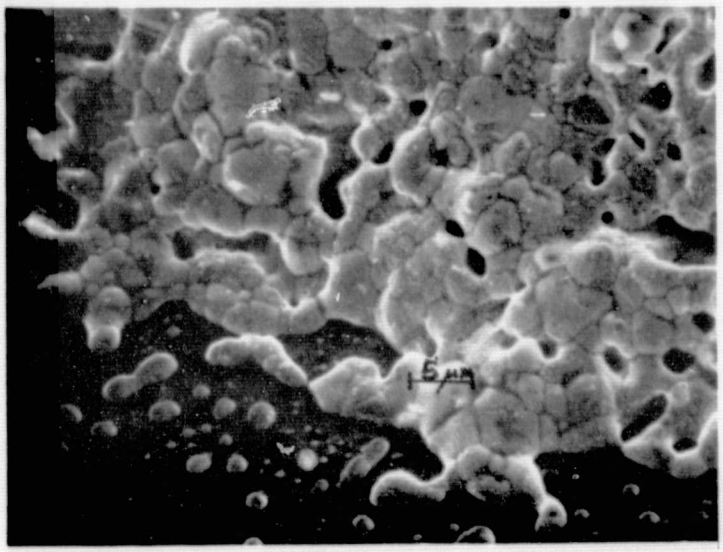

Figure 18. Same as Figures 17 and 16 except magnification 1700X. Note contiguous grain showing dense sintering.

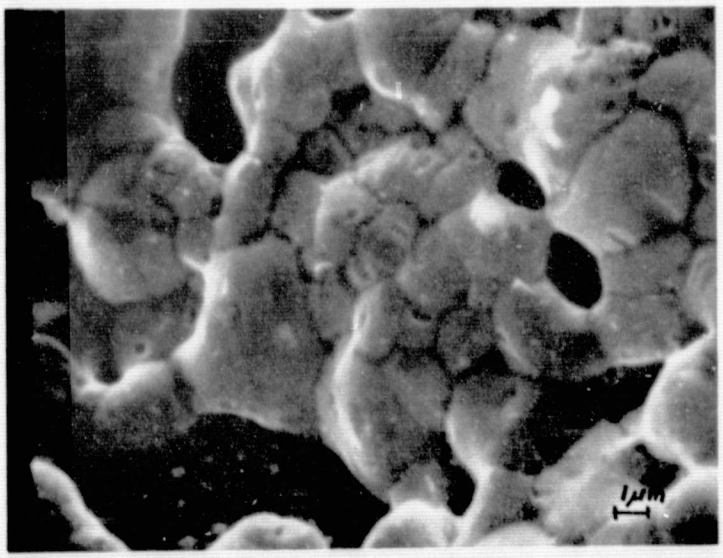

Figure 19. As above except magnification 4200X. Well-knit structure.

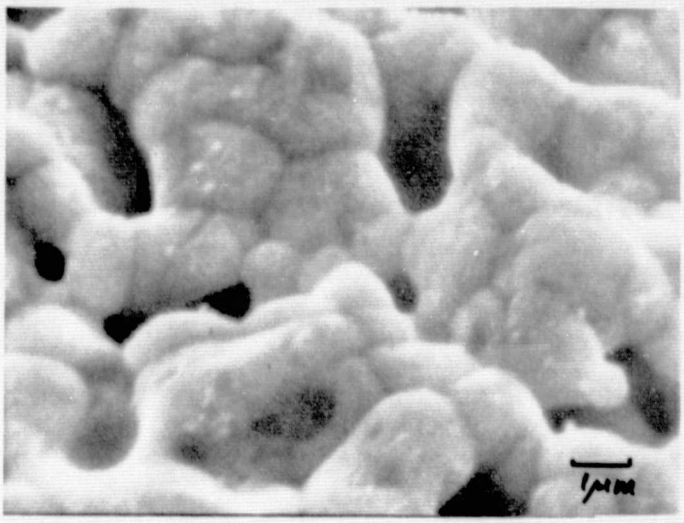

Figure 20. Solar cell metallization with conventional fritted silver ink done with Cambridge SEM at 8000X magnification.

A number of temperature runs were made on S018 (5 wt.% AgF, 3 wt.% H_3BO_3) to observe sintering action and attendant grain growth as a function of temperature. The belt speed was held constant throughout the experiment and previously printed wafers were fired at 50°C intervals from 500°C to 750°C. All specimens were analyzed with an SEM at 3000X magnification. Unfortunately, a malfunction in the SEM produced images of poor quality, but the salient features of the effect of temperature increase on the grain size and fit are strikingly shown in Figure 21.a,b,c,d,e and f. It is shown that there is an apparent reversal at 750°C in the trend in going from Figure 21.a at 700°C to Figure 21.f at 750°C. Since it is unlikely that the samples were interchanged, it is assumed that the grain size was in saturation, and the anomaly is due to local variations in screening parameters - possibly a site near the edge of a pad.

While this may be another example of a matured, all metal, sintered contact, it is possible that the boric acid doping agent serves the dual function of doping agent and non-metal (borosilicate) liquid sintering medium. This comes about due to the large ratio in densities of silver/boric acid which increase the atomic percentage to 22 wt.%.

(a)

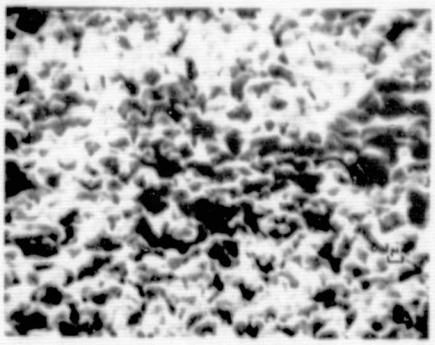

(b)

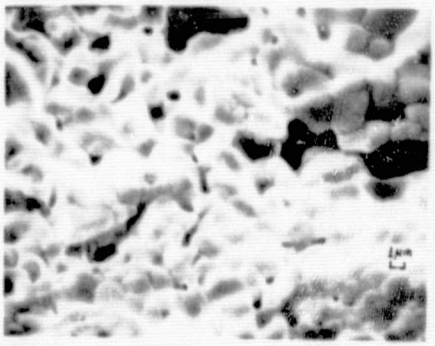

(c)

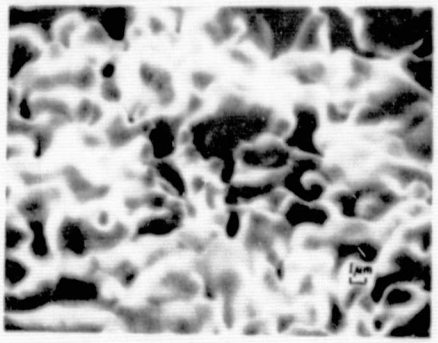

(d)

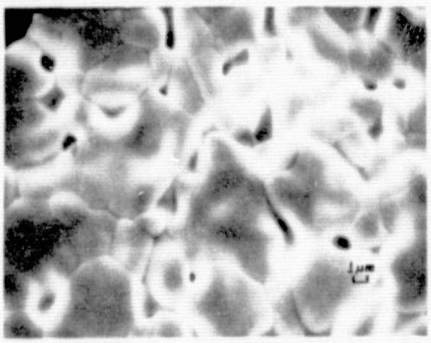

(e)

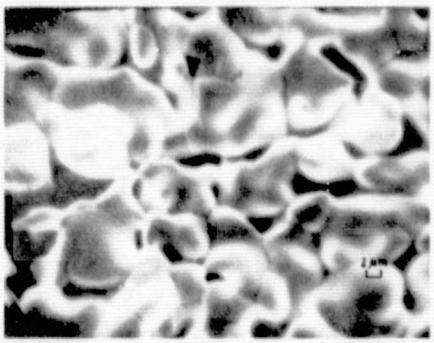

(f)

Figure 21. a) Paste S018 (with 5 wt% AgF and 3 wt% H_3BO_3) on silicon substrate, magnification 3000X, belt speed 12 cm/min, fired at 500°C b) same as (a) except fired at 550 C° c) same as (a) except fired at 600°C d) same as (a) except fired at 650°C e) same as (a) except fired at 700°C f) same as (a) except fired at 750°C.

11.2 Low Temperature Liquid Phase Sintering

Experiments in the second half of the contract period show that a quantity of 2 wt.% of silver fluoride is adequate to obtain good scratch resistant, adherent contacts.

Several inks were compounded with low melting point metal powder additions in order to attempt to lower the maturation temperature by liquid phase sintering. These include inks with 5% addition of tin powder (S021), 5% addition of lead powder (S019) and 10% addition of lead powder (S020).

These inks were fired at 500°C, 550°C, 600°C and 650°C - both in air and in nitrogen. Even the material with the smallest grain size (S019) fired in nitrogen at 500°C showed good grain structure and definite sintering. As expected, the grain size increases as a function of temperature. This can be seen in Figure 22 which shows the 5% lead addition in the left column (A) and the 10% Pb ink in column (B). Tin-containing ink (S021) gave no evidence of sintering prior to 650°C. None of the tin-containing specimens gave an adherent electrode. Since the scanning electron-micrographs of the tin-containing layers (S021) did not show much change with temperature, none of the micrographs are reproduced here. Figure 22 B top, with a micrograph of the 10% lead-containing ink (S020), shows a small amount of superstructure on the silver grains. It was thought that this might be due to a precipitated lead phase above the solid solubility of lead in silver. One such subgrain was picked for X-ray fluorescence analysis. The SEM electron beam was centered on the grain which was approximately one-third of a micron in diameter.

The lead (L_α) line lies at 10.55 keV. No evidence of lead could be found at this position above the general background radiation. The photomicrographs show the inks fired at 550°C. Additional sintering and grain growth have occurred, as might be expected, and the precipitated substructure is more in evidence. In addition to the generally increased grain growth, the higher lead percentage at 650°C shows well-developed rod-like subgrains of the precipitated phase.

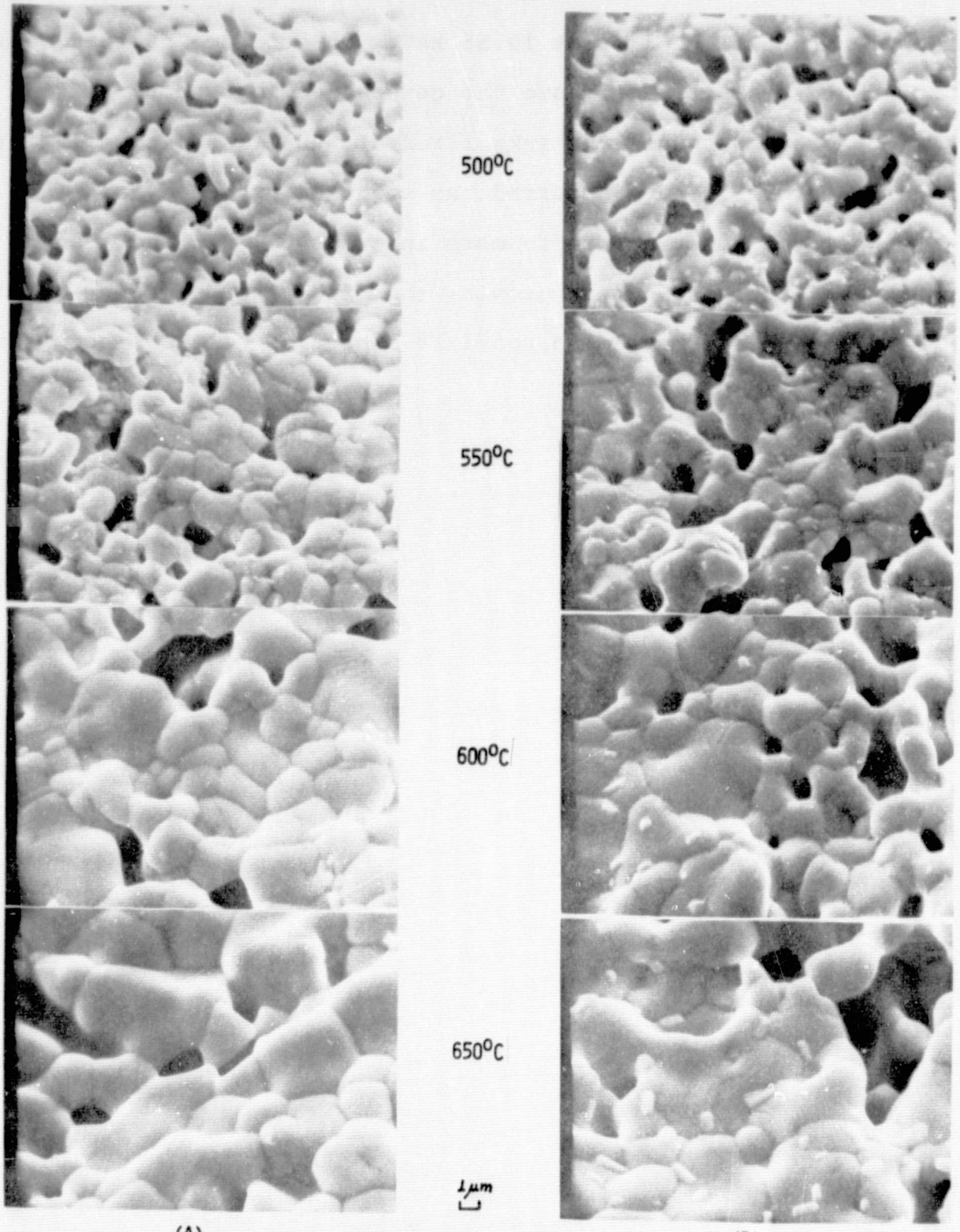

Figure 22 SEQUENCE OF PHOTOMICROGRAPHS TAKEN ON CAMBRIDGE SEM AT 5000X MAGNIFICATION OF (A) S019 PRINTS WITH 2% AgF + 5% Pb
(B) S020 PRINTS WITH 2% AgF + 10% Pb
FIRED AT THE INDICATED TEMPERATURES IN NITROGEN

BERND ROSS ASSOCIATES 4/197[illegible]

The electron beam was again focused on one of these structures and another X-ray fluorescence spectral scan was made. In this case definite evidence of the lead was detected. This is illustrated in Figure 23. In addition to the line underneath the cursor (lead L_α), the M_α line is shown well-developed near the origin at 2.35 keV. It is believed that the previous attempt to detect the lead in the small subgrain failed in view of the short absorption path ($\sim$0.30μm) available to the beam electrons within the lead crystal. This simply produced an inadequate number of X-ray photons of characteristic energy to allow detection. In the case of air sintering at 500°C, grain growth is further advanced than the equivalent nitrogen-fired sequence. It appears the air-firing lead to sintering that is equivalent to that in nitrogen at approximately 50°C higher temperature. (See Figure 24)

Figure 25 shows a set of curves plotting average grain diameter versus reciprocal temperature. Curves were plotted for four different ink compositions. The average grain diameter was obtained by measuring all the grains in a given field of the SEM image. At least thirty grains are involved in each data point on the curve. The curves approximate straight lines reasonably well. It can also be seen that the lead addition aids the sintering process at low temperatures.

The ink containing the boric acid additive described in Section 11.1 shows a break in the sintering action between 500°C and 600°C. Since anhydrous boric oxide (B_2O_3) melts at 577°C, the discontinuity may be due to a transition from solid to liquid phase sintering.

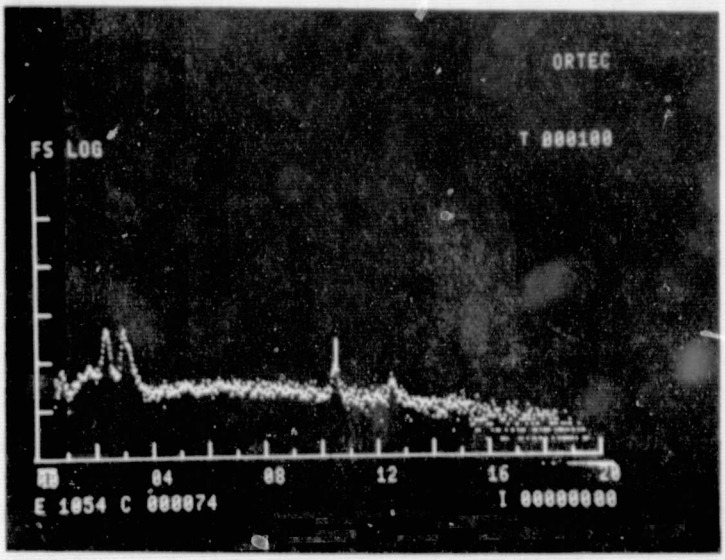

Figure 23. X-ray fluorescence scan of subgrain of S020 print at 650°C at 5000X. NOTE: Pb_{L_α} line at 10.55 keV and Pb_{M_α} line at 2.35 keV.

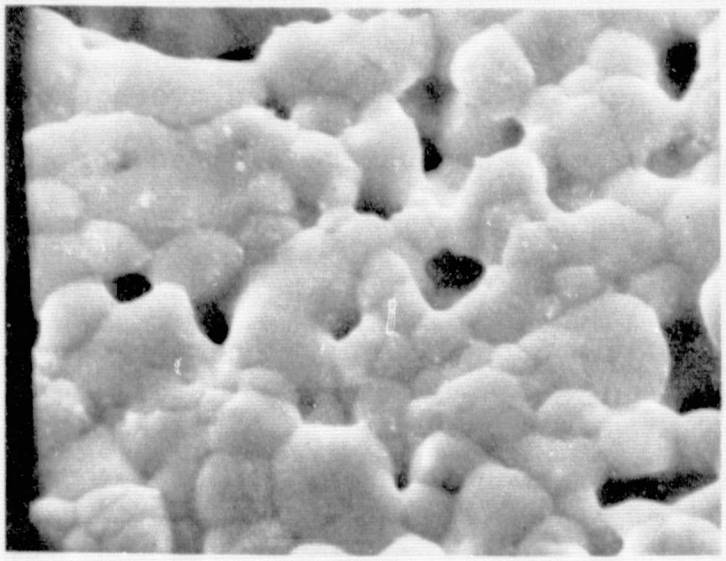

Figure 24. S019 print 2% AgF + 5% Pb fired at 500°C in air Cambridge SEM 5000X.

Figure 25

Average grain diameter variation versus reciprocal temperature for several all metal inks.

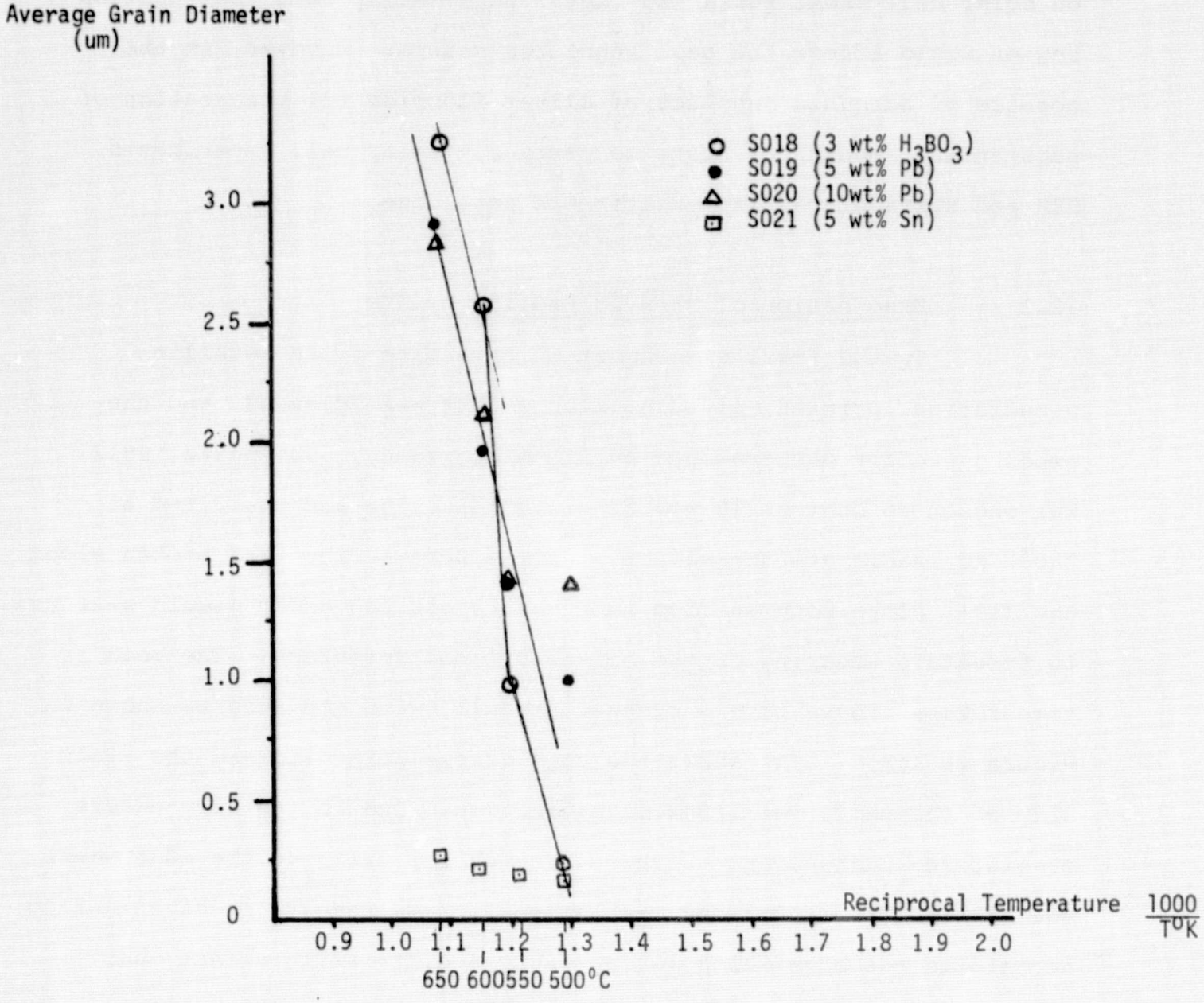

BERND ROSS ASSOCIATES

4/79

12.0 ATTACK OF SILICON SURFACE BY SILVER FLUORIDE

The most direct and product-oriented way to determine macroscopic penetration into the silicon surface would be the use of the material on solar cell front surfaces. Metal penetration into the junction region would affect the cell shunt resistance. However, in the absence of adequate supplies of silver fluoride for preparation of substantial amounts of paste to carry out solar cell experiments, SEM and surface scanning experiments were done.

12.1 Examination of Cleaved Profile by SEM

In the first experiment to determine gross metallic penetration, printed, fired silicon wafers were cleaved, and the exposed profile was examined by SEM micrography. The paste, S012, was chosen to contain 10 wt% of silver fluoride and was fired at 750^{0}C to exaggerate the effect. Wafers were scribed and broken along the (111) plane,both in room temperature air and under liquid nitrogen, to forestall smearing of the silver-silicon interface. The room temperature cleave gave a cleaner profile, with the results shown in Figure 26 A,B,C. (A) shows the edge of the print (toward the right side of the photo) at 1150X magnification. Due to the lacy nature of sintered paste contacts there are several areas at the edge where the silicon is not covered with silver. This results in highlighting or haloing the edge which is, in fact, a diffraction effect, but cannot be ascribed to a penetration since the silver fluoride is specifically absent from those areas.

The rectangle in Figure 26A shows the portion enlarged in Figure 26B and 5700X. An empty spot exists at the lower left extreme of the

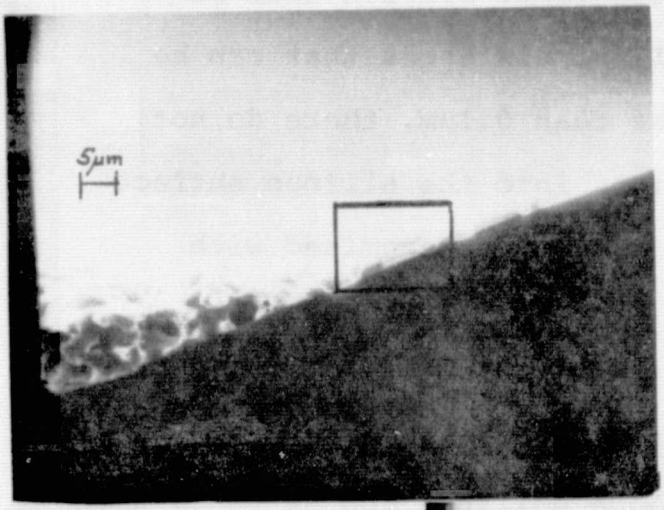

(A) 1150X MAGNIFICATION

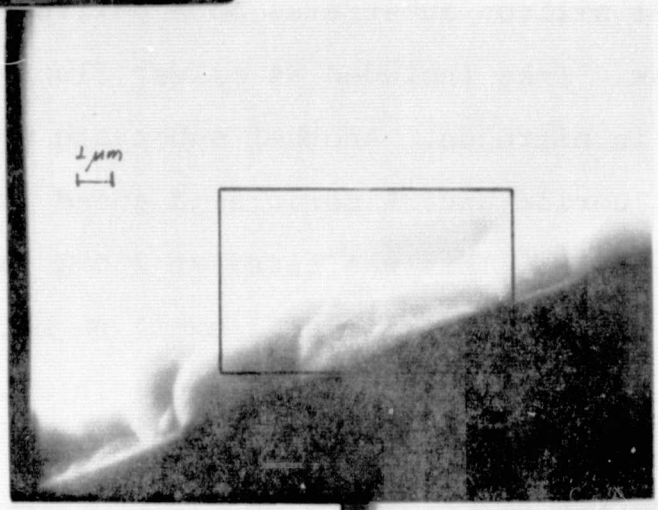

(B) 5700X MAGNIFICATION

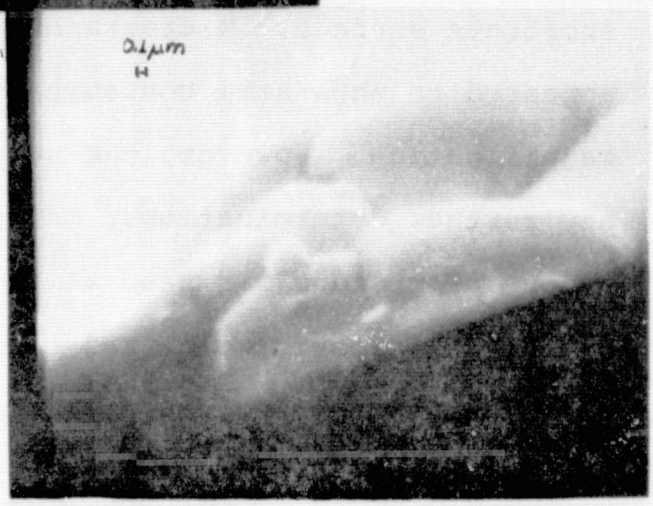

(C) 11,500X MAGNIFICATION

Figure 26

PROFILE OF ROOM TEMPERATURE CLEAVED S012 PRINT (10% AgF) ON SILICON, FIRED AT 750°C, TO DETERMINE GROSS METALLURGICAL PENETRATION INTO THE SURFACE

photo. Similarly, a rectangle shows the field of view seen in Figure 26C at 11,500X. Since the smallest distances that can be clearly resolved in this photo are less than 0.1μm, there do not appear to be any macroscopic penetrations into the silicon surface in the vicinity of the pad. Ten such areas were examined with similar results.

12.2 Examination of Printed, Nitric Acid Leached Surfaces by SEM

Several silicon substrates both polished and as sawed were screened with ink. Inks included 5% silver fluoride (S019) fired both in air and in nitrogen. Another substrate was screen-printed with 5% silver fluoride and 3% boric acid added to the master paste ink to formulate S018. This was fired at 750°C in air. All the substrates were etched in nitric acid until no metal remained. The substrates then underwent SEM micrography. In all cases, the screened acid treated areas looked darker to the eye than the remaining substrate surface. Micrographs of the printed, sawed surfaces appeared to show some contamination of the rough surface at 900X magnification. However, the surface texture was too rough to allow any further determination. On polished substrates a considerable amount of residue was seen at the periphery of the prints in the case of the S018 (boric acid) and the S009 ink. The residues appeared white under the electron microscope, an indication of high reflection or copious emission of secondaries, indicative of either a high Z (metallic surface) or a dielectric undergoing charging by the electron beam. The nature of this residue remains to be determined.

On the polished specimen, some surface structure could be observed.

In order to determine whether this structure represented hillocks or depressions, several different exposures were made with different sample tilt angles. These are shown in the following photographs. Figure 27 shows a print of S009 (5% silver fluoride and silver, fired at 750°C in air) at 4300X magnification and at a tilt angle of 45°. A number of crater like circular areas can be seen going in size from approximately one-half to two microns. The sample was tilted so as to obtain an angle of 15° for the second exposure done at a comparable magnification (4150X). It was felt that the highlighting expected from glancing beam angles on sloping surfaces might yield the looked-for information. As can be seen in Figure 28, this did not happen. Figure 29 shows the same beam angle and sample at a magnification of 8200X. Figure 30 at a comparable magnification shows a sample held at a tilt angle of 5°. The photo is largely out of focus as only a very narrow zone would be expected to produce a sharp image at such a high angle. Beyond that, no further information was gleaned from the last two figures.

A stereoscopic pair of electron micrographs was taken at a magnification of 5000X with an angle of 6.5° between pictures. These were then examined with stereoscope and while some structure was in evidence, regions appeared relatively flat and whether the structure was an artifact of chemical attack remained a mute point.

The first sample with a print of S009 was used for a profilometer scan. This is shown in Figure 31. The sensitivity of the Gould profilometer for this run was 20 microinches per division. As far as the scan is concerned, the surface may be defined as the straight sloping line.

Therefore the downward impulses can be interpreted as depressions. The deepest of these is approximately 3 1/2 divisions which would correspond to 70 microinches. Since approximately 40 microinches correspond to one micrometer, the depression would be approximately 1.75 micrometers deep. There is however, no guarantee that the surface of this portion of the wafer was level prior to the screening.

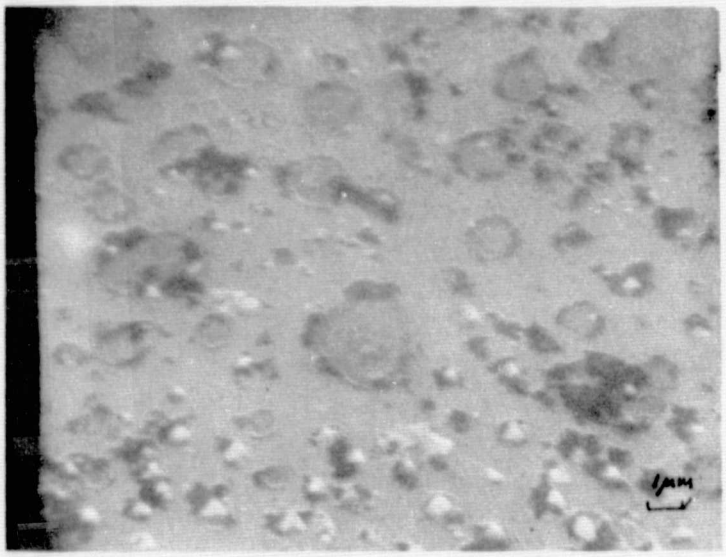

Figure 27. S009 (5 wt% AgF) on polished silicon fired at 750^{0}C in air, removed with HNO_3. Beam-sample angle 45^0 at 4300X.

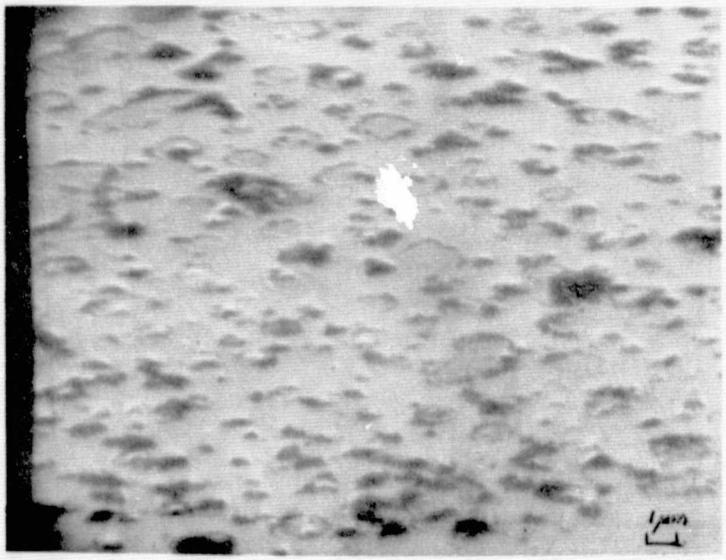

Figure 28. S009 (5 wt% AgF) on polished silicon fired at 750 C^{0}in air, removed with HNO_3. Tilt angle 15^0 at 4150X.

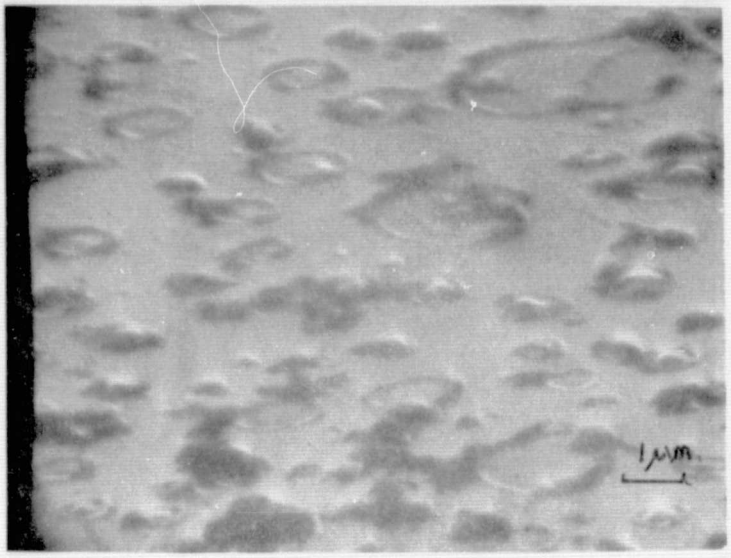

Figure 29. S009 (5 wt% AgF) on polished silicon fired at 750°C in air, removed with HNO_3. Tilt angle 15° at 8200X.

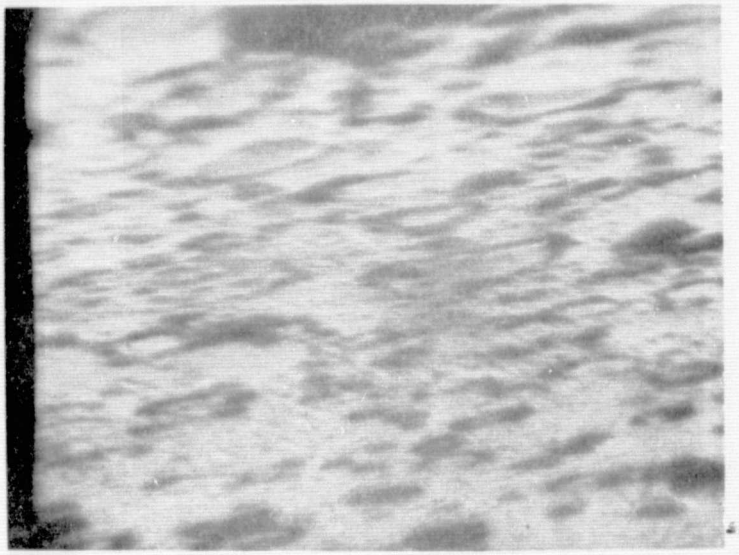

Figure 30. S009 (5 wt% AgF) on polished silicon fired at 750°C in air, removed with HNO_3. Tilt angle 5° at 9000X.

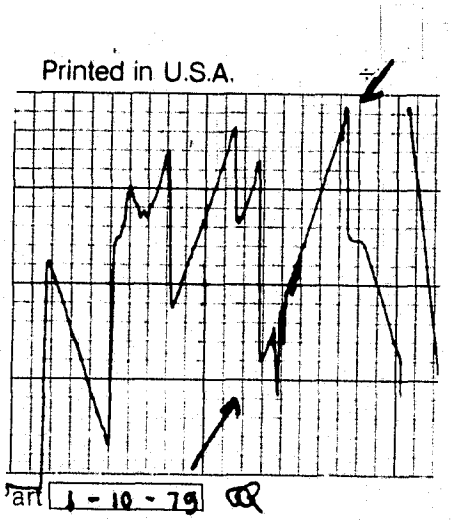

Figure 31. Gould Profilometer scan on S009 (5 wt% AgF) print on polished silicon fired at 750°C in air. Removed with HNO_3. Calibration 20 micron inches per division.

13.0 AUGER ELECTRON SPECTRA

In order to determine the nature of the interface between the silver fluoride derived silver and silicon surface, an Auger electron analysis was run. The apparatus employed a 3keV primary electron beam, with Auger electrons emitted from the sample, focused upon an electron multiplier by a cylindrical electrical field and an axial magnetic field. The electrical field was ramped from 0 to 3000V and modulated with an A.C. voltage of 3 volts below 700 eV energy and 6 volts above. Initial traces are shown in Figure 32. The second trace gives the spectrum obtained with the primary beam on the silicon surface (not near or under an electrode). The upper trace shows the spectrum obtained from the undisturbed surface of the silver contact dissociated AgF. Some sulfur, carbon, fluorine and sodium can be seen. The apparatus has provisions for etching the sample with an ion beam of argon, giving an etch rate of about 50Å/min. The third trace resulted after Ar^+ etching for 90 seconds, corresponding to a depth of 75Å into the silver. Both silicon and silver gave strong lines. No fluorine and fluorine compound could be seen. A surprise was the appearance of rhodium, scaling with silver. Figure 33 shows a profile giving relative concentration of species versus depth below the silver surface. This figure was obtained by plotting the data from 14 traces with appropriate corrections for gain and scale changes. The abscissa is broken in order to allow display of data after long term ion etch. The discontinuity in the carbon profile is due to a two-hour dwell after the 75Å etch. Apparently carbon redistributes on the surface, showing its preference for a freshly etched adsorption site.

While it might be supposed that the failure to detect an interfacial compound does not necessarily mean it is not there, this supposition is probably incorrect. In previous work with silicon reported by Chuan C. Chang[7] it was shown that silicon dioxide layers as thin as one-half monolayer can be seen by Auger spectroscopy. The effect of the oxidation bond upon the Auger line of silicon is to modify the low energy region in proximity of the line, and a similar effect would be expected in the case of a potential silicon-fluorine compound. For this reason we have confidence that the interface between silicon and silver fluoride derived silver is relatively simple.

PHYSICAL ELECTRONICS INDUSTRIES
AUGER CHART 107200

Figure 32
ACTUAL TRACE OF AUGER ELECTRON SPECTRAL YIELD FROM SURFACES NEAR THE DISSOCIATED SILVER FLUORIDE-SILICON INTERFACE

(COURTESY DR. DON SNOWDEN, IRT CORPORATION)

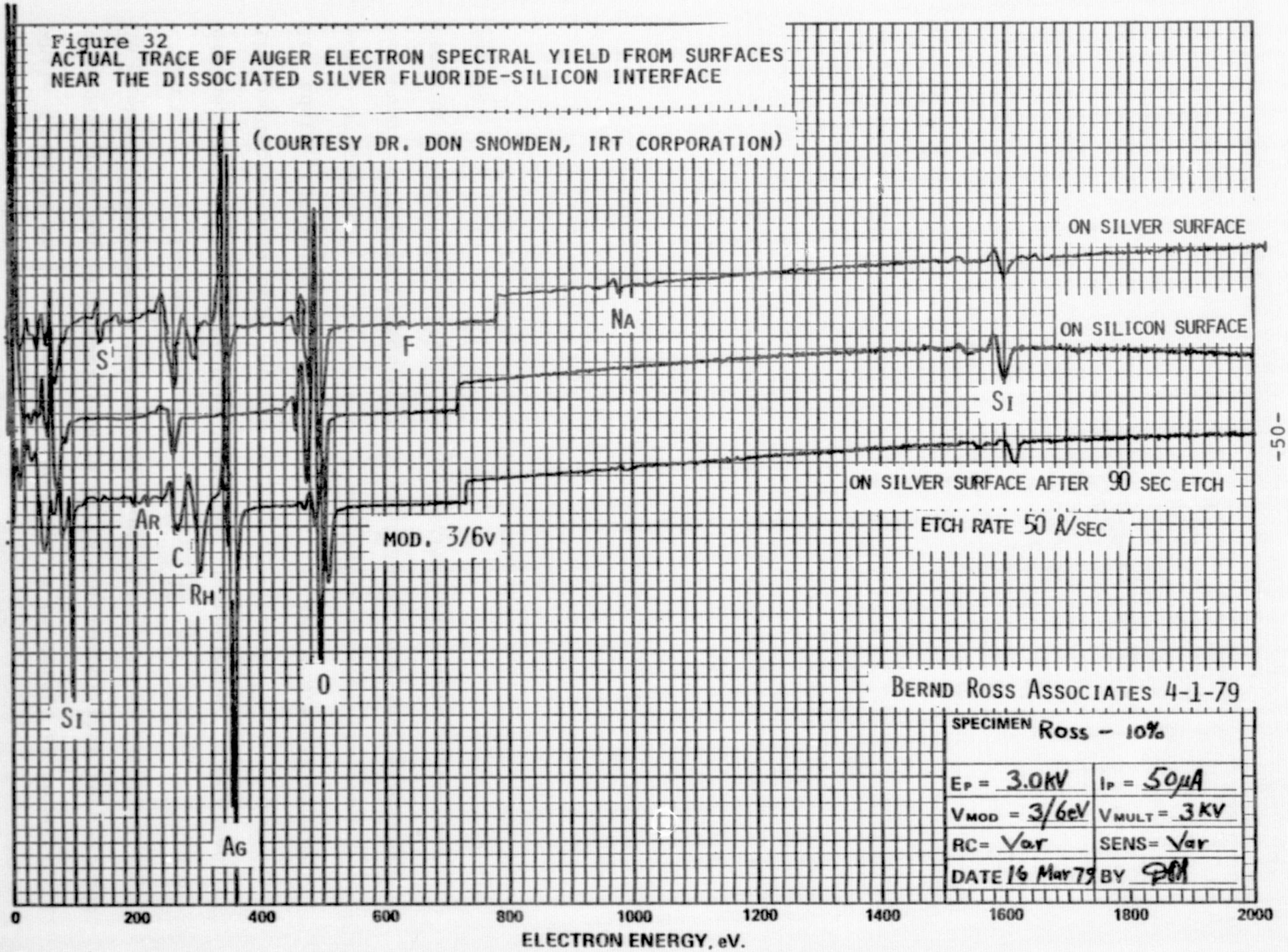

Figure 33

AUGER SURFACE SPECTRA VERSUS ETCH DEPTH

OF DECOMPOSED AgF-Si INTERFACE

(DATA COURTESY DR.DON SNOWDEN, IRT CORPORATION)

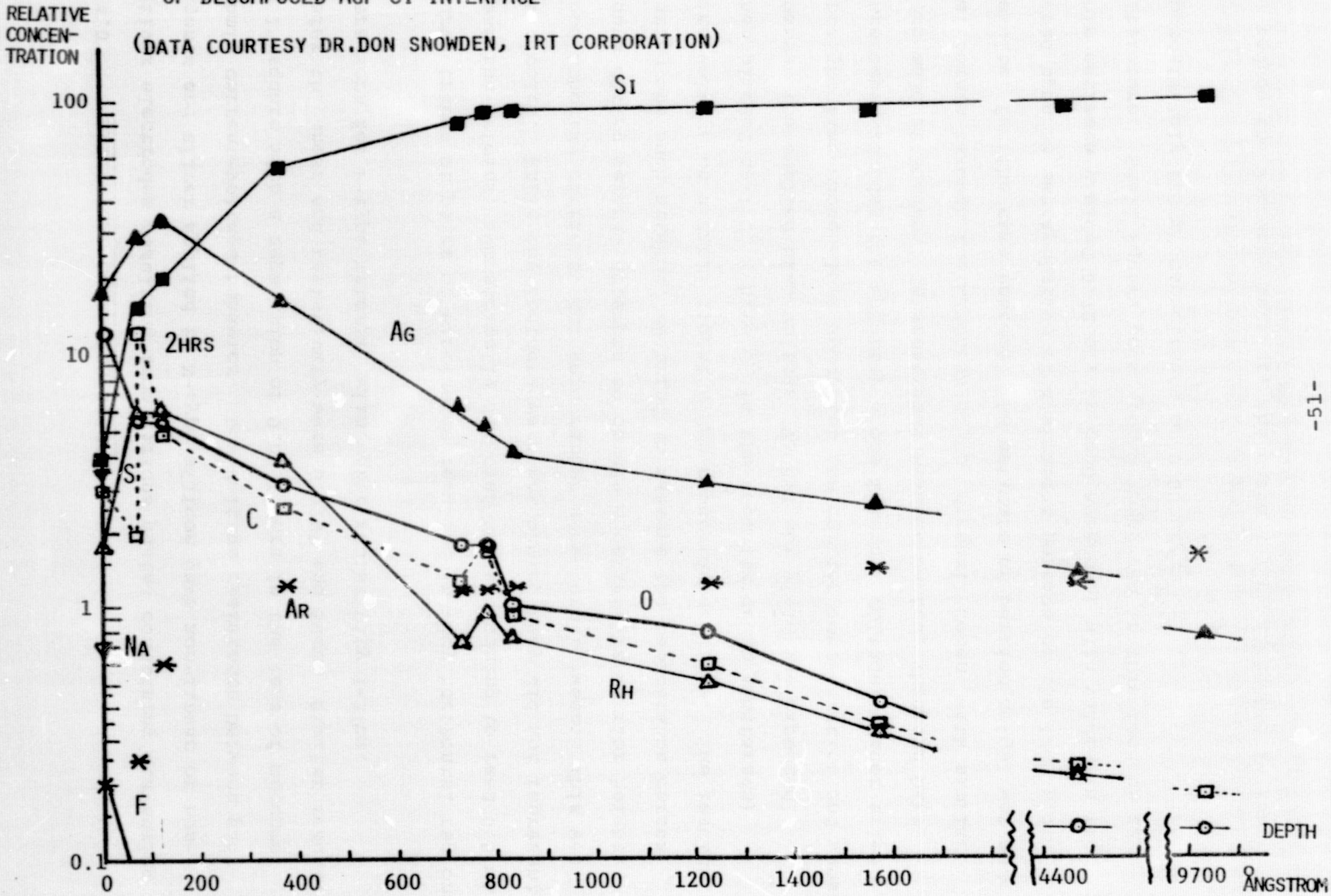

BERND ROSS ASSOCIATES, 4-1-79

14.0 ELECTRICAL CHARACTERISTICS

Silver electrodes resulting from various pastes containing scavenging agents and silver applied to N-type silicon gave non-linear or non-ohmic current-voltage behavior. Low voltage resistance between pads 0.1" square with a separation of 0.050" were in the tens of megohms. Wafer thickness and resistivity were 0.020" and 5Ωcm. Similar results were seen for P-type material with wafer resistivity 1-3Ωcm.

Curve traces of pairs of electrodes resulted in very horizontal regions near the origins, symmetrically disposed and steepening to read 0.5 mA at 4 volts. While the contacts were not ohmic, they did not represent good Schottky barriers, but were rather somewhere between. This was found during several attempts to obtain a definitive barrier height. During one such attempt, we tried to measure the capacitance versus bias voltage on a small signal 1 MHz capacitance bridge. The results, when plotted as $1/C_V^2$ (where C_V is the capacitance in picofarads) against the applied bias voltage (V), did not yield the expected straight line, whose slope specifies the carrier concentration and whose intercept provides the Schottky diode internal voltage. Other tries were made at Rockwell International Science Center, Thousand Oaks, California through the kindness of Dr. Marshall Cohen, with similar results, for the same reasons. An estimate of barrier height was made based upon an extrapolation of a straight portion of the $1/C_V^2$ plot. This estimate yielded 0.72 eV, in good agreement with values in the literature. Small square pads $(.05cm)^2$ measured in this fashion gave approximately 120 pF capacitance or 0.05 $\mu F/cm^2$.

To reduce the Schottky barrier, the paste (S018) discussed in the

previous section was prepared with 3 wt% boric acid. While there was a considerable reduction in the contact resistance to P-type substrates, the contact was still not ohmic and results were not reproducible.

Doping experiments with antimony powder gave prints with a speckled discoloration which was probably due to oxidation. Prints were fired in a reducing atmosphere in order to decrease the oxidation probability. In most of these attempts (tried with several pastes) the print lifted off the silicon surface. This was interpreted as the result of the reduction of the silver fluoride by hydrogen without the participation of the silicon dioxide. It is therefore our conclusion that a good neutral atmosphere is required, to lower the tendency to oxidize, while still allowing the silver fluoride derived nascent fluorine to perform its function on the silicon dioxide.

Several experiments with individual dopants did not yield the expected reproducible low contact resistance. It was, therefore, postulated that electrical dopant activation by diffusion was unlikely at the low temperatures employed (450°C - 700°C) and that good electrical contacts would require the creation of a thin silicon regrowth layer. This means that eutectics must be formed,consisting of an α phase of silicon and a β phase of a doping metal.

A further reduction in contact resistance was felt to be achievable, if germanium would be used to replace silicon in the α phase. This substitution has two potentially beneficial effects. The melting point of the eutectics of germanium with the metals is generally lower than that of silicon. The second advantage is the lower energy gap of germanium which aids the tunneling probability of carriers.

A number of pastes were therefore prepared with a germanium powder constituent. (See Section 17, Appendix A2 for ink formulations S042 and beyond.)

14.1 Solar Cell Experiments

Three experiments were performed with contacts screened on solar cells. This work was done on the premises of Optical Coating Laboratories, Inc. (OCLI). In the first of these, inks S032 (neutral), S033 (0.5% Al), S034 (0.1% Sb) and S035 (0.1% B) were utilized in conjunction with a commercial control paste with glass frit (Owens-Illinois OI 6103). In order to obtain the most information, partially completed solar cells were using having (a) evaporated Titanium-Silver (Ti - Ag) front contacts and screened backs, (b) Ti - Ag back contacts and screened front contacts and (c) cells in which both front and back contacts were screened. After screening, cells with prints were dried at 250°C and fired at 650°C in nitrogen or in hydrogen. Best curve shapes were obtained with evaporated Ti - Ag backs and screened front contacts, and poorest characteristics resulted when both front and back were screened with the same ink. Results from the control ink were equally bad. The major problem appeared to be the contact resistance of the screened electrodes, while front surface junction shunting did not appear to be a serious problem.

In the second solar cell experiment three inks were tested; S050 (1.54% $GaCl_3$), S051 (0.45% $GaCl_3$ + 1.17% Ge) and S052 (0.24% Al + 1.17% Ge). Prints were dried as before (250°C) but two firing temperatures were used, 550°C and 650°C. In this experiment starting

cells had either evaporated front (Ti - Ag) contacts or evaporated back contacts. Curve shapes were somewhat improved over the first experiment particularly the front screened cells fired at 550°C, and back screened cells fired at 650°C. It appeared that considerable junction shunting occurred with these inks at 650°C on the front surface, and that the back contact resistance could be improved by increasing the temperature.

At this point some eutetic powder containing pastes had been prepared. These included S057 with 5% Al - Si eutectic, S058 with 5% Al - Ge eutectic and S059 with 5% Al - Ge eutectic + 1% $GaCl_3$. Experiments with silicon blanks had shown that the lowest resistances between screened electrodes were obtained at firing temperatures of 650 C and 700 C. In the last solar cell experiment that was carried out, the format was similar to Experiment I but only enough cells were available for a single temperature, and 700°C was chosen. Unfortunately this temperature was sufficient to cause severe junction shunting in all cells, also in an evaporated Ti - Ag control cell.

14.2 Experiments with Specific Contact Resistance

After electrical measurements were begun, it became obvious that the simple electrode patterns employed, gave measurement results which did not allow accurate assessment of the specific contact resistance. Measurements to this point consisted of Kelvin probing adjacent square pads on silicon and involved knowledge of silicon resistivity and current paths. A method of measuring contact resistance was found which proved to be highly suitable for screened contacts. A current source and sink contact are applied to the

semiconductor wafer or layer, and a number of narrow contact lines are disposed between the current contacts. The contact lines are placed at regular intervals between the current electrodes and are conveniently dismensioned to allow voltage probing. The measurement is done by allowing a constant current to flow through the current terminals, while successively probing the contact lines with a high impedance voltmeter. When plotting the voltage versus distance, a negative intercept results when extrapolating the straight line portion of the curve towards zero voltage. The specific contact resistance can then be calculated from

$$r_c = L_T^2 R_\square$$

where $r_c \equiv$ specific contact resistance in Ωcm^2

$L_T \equiv$ transfer length (x axis intercept) in cm

$R_\square \equiv$ sheet resistance in ohms/$\square$ (slope of curve)

The sheet resistance is

$$R_\square = \frac{\Delta V_x}{I} \frac{Z}{L}$$

$\Delta V_x \equiv$ voltage drop along L in volts at a current $I_{(amps)}$

$L \equiv$ distance in cm

$Z \equiv$ width of one square in cm

This method is due to Shockley and is described in Reference 8.

Screen masks were designed and fabricated to facilitate testing of inks and processing parameters in terms of specific contac-resistance. Masks were completed during the preparation of this report and only preliminary measurement results can be reported.

Current source and sink electrodes are squares of 0.100 inches

edgelength. The voltage probing electrodes are spaced on 10 mil (25μm) centers and are 10 mil (25μm) wide.

Initial results indicate the pastes with eutectic powder additives to have contact resistances in the range of $5 \cdot 10^{-4} \Omega cm^2$ to $3 \cdot 10^{-3} \Omega cm^2$ with relative tolerance to firing temperature. Best results were obtained with a paste containing a commercially available aluminum - silicon eutectic powder. Variability in results from eutectic powders prepared at our facility is probably due to preoxidized powders and potential oxygen contamination of our furnace atmosphere.

15.0 CONCLUSIONS, PROBLEMS AND RECOMMENDATIONS

The concept of a fritless ink for use on semiconductor materials, specifically on silicon, has been shown to be feasible. Three solid phase etchants which can be incorporated in the pastes have been identified. The best of these, silver fluoride, leaves behind as its only residue a finely divided metallic silver powder which facilitates wetting the silicon surface and accelerates the sintering action due to the catalytic effect of the small particle size. Auger Spectrometry has shown the absence of any silicon-fluorine chemical combinations at the silicon-silver interface which might pose a potential threat to reliability or operating life of the contact. Metallurgically the resulting contact is excellent, based on examination of structural electronmicrography, adhesion, scratch resistance and solderability. The contact has been subjected to boiling in DI water for 1 hour without any loss of adhesion or scratch resistance. The bulk requirement of silver fluoride in the preparation of inks is modest with 2 wt% being sufficient to retain the above qualities.

The temperature range of processing for the all metal ink was decreased from an initial 700°C - 750°C to 500°C - 600°C by the addition of a frit-metal which serves as a liquid phase sintering medium during electrode maturation.

Problems in obtaining product meeting specifications at quoted delivery times have recently been eliminated, and therewith the need to embark on a silver fluoride manufacturing project.

Solar cells with adequately low contact resistance and simultaneous

prevention of junction shunting has not been accomplished, but pastes containing semiconductor-doping metal eutectic powders show considerable promise. Most recent data, as yet unconfirmed, resulting from a convenient method for contact resistance measurement, indicate contact resistances in the order of 1 $m\Omega cm^2$ for the eutectics.

The lack of adequate furnaces/furniture to provide forming gas/hydrogen or uncontaminated neutral furnace atmospheres at the present facility is a potential problem, and is being dealt with.

RECOMMENDATIONS

It is recommended that work be instituted leading to an optimized, screenable all metal silver paste electrode. The investigation should involve process parameters and ink composition, with optimization of contact resistance, sheet conductance, solder leach resistance, tolerance to temperature-humidity cycles and prevention of junction shunting.

Similarly screenable all metal inks should be developed, having as their major constituent a base metal, such as nickel or copper, leading to an optimized low cost electrode system.

16.0 PROGRESS ON PROGRAM PLAN

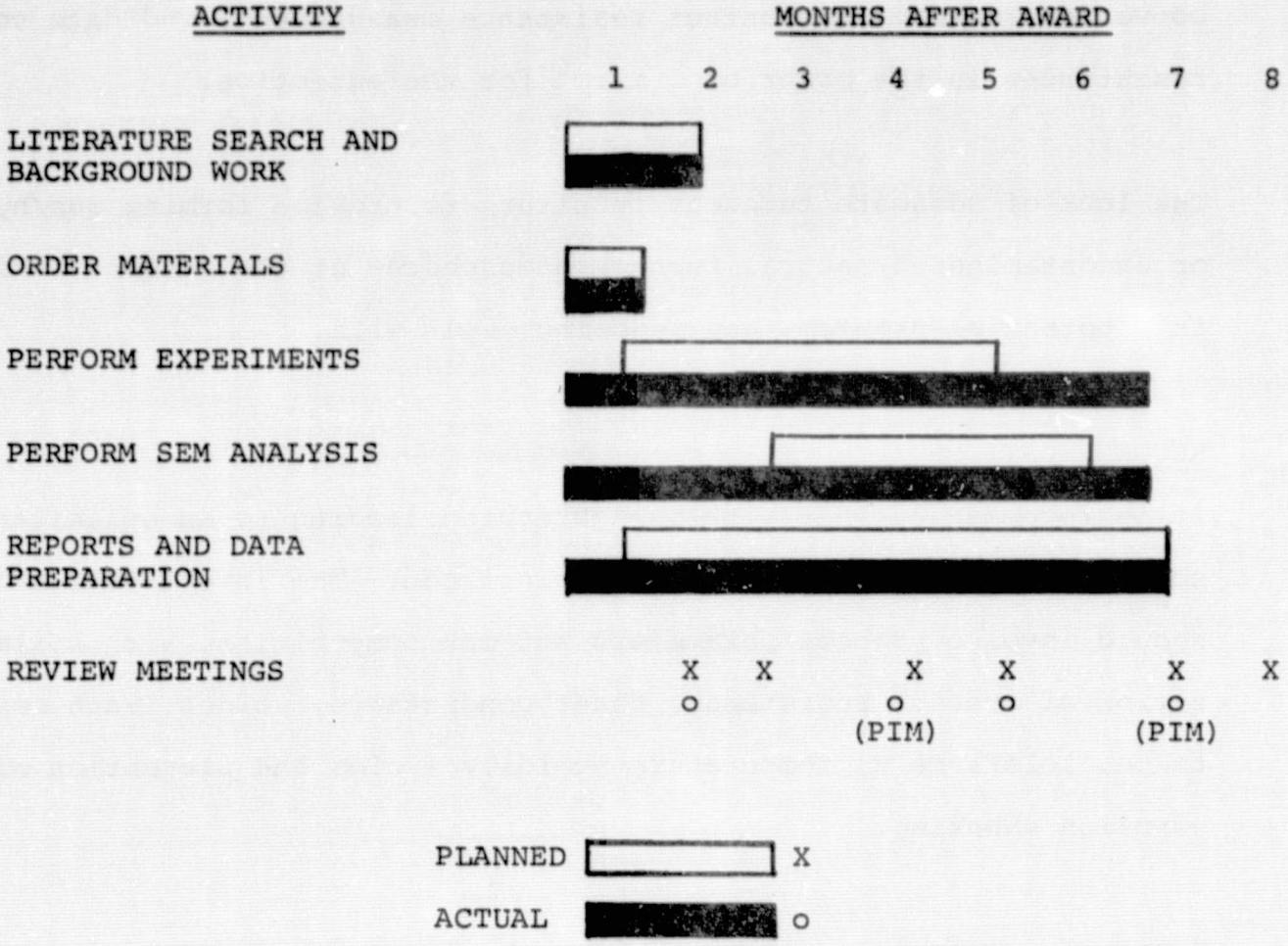

17.0 APPENDIX

A.1 SYNTHESIS OF SILVER FLUORIDE

Due to procurement problems the possibility of synthesizing the silver fluoride at the site of the subcontractor was entertained. Manufacturing methods taken from the literature are described in the following paragraphs.

Silver fluoride may be fabricated by dissolving freshly precipitated silver carbonate (Ag_2CO_3) or silver oxide (Ag_2O) in hydrofluoric acid and evaporating the solution. The difficulty with this process, as described by H. Moissan[9] and A. Guntz[10], arises in the purification of the raw product or in the removal of the last H_2O rests. During recrystallization from H_2O, some silver fluoride hydrates are produced which are difficult to dehydrate. When the evaporated reaction mixtures or the hydrates are dried through heating at higher temperature a silver oxide and silver metal contaminated product results.

The reaction product which is achieved by an evaporation of the solution of silver carbonate in 40% hydrofluoric acid and by subsequent heating up to 200°C - 250°C contains 92-95% silver fluoride, 5-8% silver oxide (Ag_2O) according to Dubrikow, et. al.[11] A similar process yields 97 1/2% silver fluoride in addition to silver oxide and silver metal according to Hayek, et. al.[12]

In order to provide a pure, water free form of silver fluoride, silver carbonate is dissolved in 40% hydrofluoric acid until saturation is obtained. The filtered solution is evaporated and stirred until crystal formation begins. Any remaining H_2O can be removed by 3 successive additions of dehydrated methanol and subsequent decanting. Next, in a similar manner, the material is washed with dry ether and the light brown to yellow powder is dried at 60-70^{0}C. Because of the light sensitivity of silver fluoride, direct exposure to light must be avoided. It may be stored in dark paraffinated vessels or in sealed polyethylene bags in dark glass bottles. A similar production process is given for silver oxide (Ag_2O) or silver carbonate (Ag_2CO_3) and hydrofluoric acid, according to K. H. Lieser.[13] He also describes the synthesis for starting with silver powder, peroxide (H_2O_2) and hydrofluoric acid.

Further purification of the recrystallized product of silver carbonate and hydrofluoric acid (Ag_2CO_3+ HF) can be obtained by adding dry benzene in quantity of three times the volume of the other constituents and by slow distillation. In this case, the H_2O comes off as an azeotropic mixture of water and benzene ($H_2O + C_6H_6$). Next the brown powder is dried in vacuum at 140^{0}C. Dehydration of the recrystallized silver fluoride hydrate during recrystallization can also be accomplished by week long dries over P_2O_5 in vacuum and absence of light. A yield of 50-60% is obtained according to F. J. Buckle.[14] Drying of the reaction product of silver carbonate and hydrofluoric acid in an HF stream is described by K. Jellinek, et.al.[15] Evaporation of the solution to dryness and addition of HF and renewed evaporation to dryness can also be done according to A. W. Jache, et.al.[16] For the

production by a completely dry method, one allows dehydrated HF to flow over silver carbonate in a platinum tube and with slowly rising temperature profile peaking at 310°C. One then allows it to cool in a dry nitrogen stream.

Completely water free crystalline silver fluoride can be produced through electrolysis of potassium fluoride dissolved in non aqueous acetic acid. A silver metal anode is utilized. The silver fluoride is formed at the anode at a current of 40 milliamps or greater and collects as a clean white, fine crystalline deposit on the bottom of the electrolysis vessel. Because of light sensitivity, the fabrication should be carried out in the dark according to H. Schmidt.[17]

A.2 LIST OF ALL-METAL ELECTRODE PASTES

PASTE NUMBER	MASTER PASTE NUMBER AND %	METAL* POWDER PM4011 %	METAL* FLAKE PM4023 %	OXIDE SCAVENGER AgF* %	METAL FRIT %	DOPANTS %
S001			5.0		Tin/ 95.0	
S002			10.0		Tin/ 90.0	
S003			98.0		Si/ 2.0	
S004			98.0	2.0		
S005			95.0	5.0		
S006			90.0	10.0		
S007			75.0	25.0		
S008		25.0	PM4016/ 75.0			
S009	S008/ 95.0			5.0		
S010	S008/ 95.0			DLX6000/ 5.0		
S011		24.97	PM4016/ 75.0			
S012	S008/ 90.0			10.0		
S013	S008/ 90.0			NH_4F/ 10.0		
S014	S008/ 90.0			DLX6000/ 10.0		
S015		22.5	PM4016/ 67.5	NH_4F/ 5.0	Tin/ 5.0	
S016		21.25	PM4016/ 63.75	NH_4F/ 5.0	Tin/ 10.0	
S017		18.75	PM4016/ 56.25	NH_4F/ 5.0	Tin/ 20.0	
S018	S009/ 97.0					H_3BO_3 3.0
S019		23.25	69.75	2.0	Lead/ 5.0	
S020		22.0	66.0	2.0	Lead/ 10.0	
S021		23.25	69.75	2.0	Tin/ 5.0	
S022	S008/ 95.0			5.0		

A.2 LIST OF ALL-METAL ELECTRODE PASTES
(Continued)

PASTE NUMBER	MASTER PASTE NUMBER AND %	METAL* POWDER PM4011 %	METAL* FLAKE PM4023 %	OXIDE SCAVENGER AgF* %	METAL FRIT %	DOPANTS %
S023		Ni/ 95.0			Lead/ 5.0	
S024		Cu/ 95.0			Lead/ 5.0	
S025		21.87	65.63	2.0	Lead/ 10.0	Sb/ 0.5
S026		23.22	69.79	2.0	Lead/ 5.0	Al/ 0.1
S027		23.22	69.79	2.0	Lead/ 5.0	Sb/ 0.1
S028		23.25	69.75	$AgBF_4$ 2.0	Lead/ 5.0	→ (also)
S029		24.47	73.42	2.0		Al/ 0.1
S030		24.47	73.42	2.0	Sb/ 0.1	
S031		24.5	73.5	$AgBF_4$ 2.0		→ (also)
S032		23.25	69.75	2.0	Lead/ 5.0	
S033	S032/ 99.36					Al/ 0.64
S034	S032/ 99.9				Sb/ 0.1	
S035	S032/ 98.8					H_3BO_3/ 1.2
S036	S032/ 98.0					TiH_2/ 2.0
S037	S032/ 98.0					ZrH_2/ 2.0
S038	S032/ 99.0					$InCl_3$/ 1.0
S039	S032/ 98.0					$InCl_3$/ 2.0
S040	S032/ 99.0					$GaCl_3$/ 1.0
S041	S032/ 98.0					$GaCl_3$/ 2.0
S042	S032/ 98.0					Ge/ 2.0
S043	S032/ 95.0					Ge/ 5.0

A.2 LIST OF ALL-METAL ELECTRODE PASTES
(Continued)

PASTE NUMBER	MASTER PASTE NUMBER AND %	METAL* POWDER PM4011 %	METAL* FLAKE PM4023 %	OXIDE SCAVENGER AgF* %	METAL FRIT %	DOPANTS %
S044	S032/ 93.0					Ge/ 5.0 $GaCl_3$/ 2.0
S045	S032/ 93.0					Ge/ 5.0 ZrH_2/ 2.0
S046	S032/ 93.0					Ge/ 5.0 TiH_2/ 2.0
S047	S032/ 93.0					Ge/ 5.0 ZrH_2/ 2.0
S048	S032/ 93.0					Ge/ 5.0 B/ 2.0
S049	S032/ 94.0					Ge/ 5.0 Al/ 1.0
S050	S032/ 98.0					$GaCl_3$/ 2.0
S051	S032/ 93.0					Ge/ 5.0 $GaCl_3$/ 2.0
S052	S032/ 94.0					Ge/ 5.0 Al/ 1.0
S053	S032/ 95.0					(Ge + Al) eu/ 5.0 in N_2
S054	S032/ 95.0					(Ge + Al) eu/ 5.0 in Air
S055	S032/ 95.0					(Ge + Ga) eu/ 5.0 in Air
S056	S032/ 95.0					(Ge + In) eu/ 5.0 in Air
S057	S032/ 95.0					(Al + Si) eu/ 5.0 in Air

A.2 LIST OF ALL-METAL ELECTRODE PASTES
(Continued)

PASTE NUMBER	MASTER PASTE NUMBER AND %	METAL* POWDER PM4011 %	METAL* FLAKE PM4023 %	OXIDE SCAVENGER AgF* %	METAL FRIT %	DOPANTS %
S058	S032/ 95.0					$(Ge+Al)_{eu}$/ 5.0 in N_2
S059	S032/ 95.0					$(Ge+Al)+Ga_{eu}$/ 5.0 in N_2
S060	S032/ 95.0					$(Al+Si)_{eu}$/ 5.0 in N_2
S061	S032/ 95.0					$(Al+Si)+Ga_{eu}$/ 5.0 in N_2

V5005 USED AS 23 WT.% IN ALL PASTES

* UNLESS OTHERWISE INDICATED

eu - SIGNIFIES EUTECTIC ALLOY POWDER

Air/N_2 - ALLOYING ATMOSPHERE FOR THE EUTETIC

18.0 BIBLIOGRAPHY

1. "Constitution of Binary Alloys", M. Hansen and K. Anderko, 2nd Edition, page 40, McGraw-Hill, New York, NY, (1958)

2. "Handbook of Chemistry and Physics", 56th edition, CRC Press, Cleveland, OH, (1975-1976), page B-138 S147.

3. Gmelin' "Handbuch der Anorganischen Chemie", 8. Aufl. Teil B3, page 146 (1973).

4. H. C. Urey, "The Merck Index", page 948, 8th edition, P. G. Stecher, Ed. Merck & Co. (1968).

5. I. A. Aksay, E. E. Hoge, J. A. Pask, J. Phys. Chem. 78, 1178, (1974).

6. K. F. Zmbov and J. L. Margrave, J. Phys. Chem. 71, 446, (1967).

7. C. C. Chang, "Characterization of Solid Surfaces", Kane & Larabee Eds, Plenum Press, page 531 (1974).

8. Hower, Hooper, Cairns, Fairman and Tremere, "Semiconductors and Semimetals", Willardson & Beer Eds., Academic Press, page 178, chapter 3, vol. 7, Part A, (1971).

9. H. Moissan, Bull. Soc. Chim., France, 5, 456 (1841)

10. A. Guntz, Ann. Chim., Paris, 2, 101 (1914).

11. L. M. Dubrikow and N. I. Sorin, Zh. Obshch. Khim., 17, 185 (1947).

12. E. Hayek, A. Czaloun and B. Krismer, Monatsh. Chem., 87, 741, (1956).

13. K. H. Lieser, Z. Anorg. Allgem. Chem., 305, 133, (1960).

14. F. J. Buckle, F. L. M. Pattison, B. C. Saunders, J. Chem. Soc., 9, 1471, (1949).

15. K. Jellinek and A. Rudal, Z. Anorg. Allgem. Chem., 175, 281, (1928).

16. A. W. Jache and G. H. Cady, J. Phys. Chem., 56, 1106, (1952).

17. H. Schmidt, Z. Anorg. Allgem. Chem., 270, 188, (1952).